A novel method to detect label-free nanoplastics within whole organisms using enhanced dark field hyperspectral imaging

Arav Saherwala

Department of Chemical Engineering

McGill University, Montreal

July 2024

A thesis submitted to McGill University in partial fulfillment of the requirements of the degree of Master of Science in Chemical Engineering

Table of Contents

Acknowledgements

I want to thank my thesis supervisor, Dr. Nathalie Tufenkji, for her guidance and expertise throughout the course of my master's. Her attention to detail and thoughtful advice has helped me overcome many challenges during this project. I am immensely grateful to my post-doctoral mentor, Dr. Jun-Ray Macairan, for his mentorship and support. His patience, optimism, and expertise have taught me valuable skills throughout my graduate studies. I would also like to thank Dr. Ana Quevedo for her help and expertise in ecotoxicology. I must also express my gratitude to Dr. Youssef Chebli at the MacDonald Campus's Multiscale Imaging Facility for his guidance on the cryotome. I am also grateful to undergraduate researcher, Emma Geoffroy. Special thanks to other members of the Biocolloids and Surfaces Laboratory for their vital contributions, for sharing their expertise, and for providing their helpful advice. Lastly, a special thanks to my family and friends, who have always been my biggest supporters.

This project was funded by McGill University through the McGill Engineering Eugenie Ulmer Lamothe Scholarship, the Natural Sciences and Engineering Research Council of Canada (NSERC) through its Pollution in Urban Environments Collaborative Research and Training Experience (PURE CREATE) program and Discovery program, Fonds de Recherche Nature et technologies through its EcotoQ program and Team Projects program, the Canada Research Chairs program, Fisheries and Oceans Canada, and the Canada Foundation for Innovation.

Abstract

Anthropogenic activities have led to most generated plastic being landfilled or introduced to the environment. Natural weathering conditions, such as exposure to UV irradiation, mechanical degradation, and temperature changes, break down plastic litter into smaller microplastics and nanoplastics (MNP). These emerging contaminants pose a hazard to the aquatic environment and life because of the risk of consumption and bioaccumulation up the food chain. The omnipresence of MNP compels researchers to better understand their transport, toxicity, and fate in aquatic environments, including freshwaters. However, nanoplastics have proven challenging to detect due to their smaller size, which has limited our understanding of their environmental impacts. This work focuses on detecting internalized MNP in a model freshwater organism (*Daphnia magna*) using a combination of histological techniques and enhanced darkfield hyperspectral microscopy. The advantage of this method is that it is label-free, meaning that the plastics do not need to be pre-labeled prior to internalization by organisms. This study presents a method to modify the spectral response of organism biomass by staining the biomass with a dye, enabling the detection of ingested MNP. This makes it a promising methodology for ecotoxicology studies since uptaken MNP can be localized inside the organism, thereby helping to understand the observed metabolic impacts. This research will aid in shaping future research on the impact of MNP pollution on freshwater systems.

Résumé

Les activités anthropiques ont conduit à la mise en décharge ou à l'introduction de la plupart des plastiques générés dans l'environnement. Les conditions météorologiques naturelles, telles que l'exposition aux rayons UV, la dégradation mécanique et les changements de température, décomposent les déchets plastiques en microplastiques et nanoplastiques (MNP) plus petits. Ces contaminants émergents constituent un danger pour l'environnement aquatique et la vie en raison du risque de consommation et de bioaccumulation en amont de la chaîne alimentaire. L'omniprésence des MNP oblige les chercheurs à mieux comprendre leur transport, leur toxicité et leur devenir dans les milieux aquatiques, y compris les eaux douces. Cependant, les nanoplastiques se sont avérés difficiles à détecter en raison de leur petite taille, ce qui a limité notre compréhension de leurs impacts environnementaux. Ce travail se concentre sur la détection de MNP internalisée dans un organisme d'eau douce modèle (*Daphnia magna*) en utilisant une combinaison de techniques histologiques et de microscopie hyperspectrale à fond noir améliorée. L'avantage de cette méthode est qu'il s'agit d'une méthode sans marquage et que, par conséquent, les plastiques n'ont pas besoin d'être prétraités avant d'être internalisés par des organismes. Cette étude présente une méthode pour modifier la réponse spectrale de la biomasse de l'organisme, permettant la détection de MNP ingérés. Cela en fait une méthodologie prometteuse pour les études écotoxicologiques, car l'absorption des PMN peut être visualisée. Cette recherche aidera à orienter les recherches futures sur l'impact de la pollution par les MNP sur les systèmes d'eau douce.

Contribution of Authors

Arav Saherwala, Jun-Ray Macairan, and Nathalie Tufenkji devised the experimental design. Arav Saherwala and Jun-Ray Macairan completed *Daphnia magna* exposures and obtained the histological slices on the cryotome. Arav Saherwala developed the staining protocol. Arav Saherwala, Jun-Ray Macairan, and Emma Geoffroy collected darkfield images, and subsequent analysis on the ENVI 4.8 software. Arav Saherwala performed the data analysis under the direction of Jun-Ray Macairan. Arav Saherwala wrote the thesis, and all co-authors reviewed all written work.

Author List and Affiliations

A. Saherwala[1], J.R. Macairan[1], E. Geoffroy[2], N. Tufenkji[1]

[1] Department of Chemical Engineering, McGill University, Montreal, Quebec, Canada H3A 0C5

[2] Department of Bioengineering, McGill University, Montreal, Quebec, Canada H3A 0C5

List of Figures

List of Tables

Chapter 1: Introduction and Literature Review

Production, Use, and Fate of Plastics

Mass plastic production and use started in the early 1950s.[1] This time period has also been marked as the beginning of the Anthropocene period,[2] where human-made processes have overtaken the Earth's natural processes.[3] Since the 1950s, approximately 8.3 billion metric tons of plastic have been produced, of which 60% was sent to landfills or the environment.[4] In 2010, it was estimated that 4.8 to 12.7 million tonnes of plastic was dumped into aquatic environments.[5] These statistics are based on coastal countries in one year. With global plastic production increasing to 460 million tonnes in 2019,[6] one can safely assume that the amount of plastics deposited into aquatic environments has only increased since 2010.[7-9]

The ubiquity of plastics stems from the broad range of industries using plastic products, for instance: consumer goods packaging (44%), construction (18%), automotive (8%), electronics (7%), household items (7%), and agriculture (4%).[10] There are five main types of plastics in circulation: polystyrene (PS), polypropylene (PP), polyvinylchloride (PVC), polyethylene (PE) which includes both low and high density, and polyethylene terephthalate (PET).[1]

Large plastic waste breaks down into smaller microplastics and nanoplastics (MNP) due to weathering conditions such as UV irradiation, mechanical fracture, biological degradation, and temperature fluctuations. The weathering of MNP contributes to morphology and property changes of MNP.[13] There are two sources of MNP: primary and secondary. Primary MNP are considered pristine micro and nanobeads; generally, they are used in cosmetics, packaging, and electronics.[12] In the environment, macroplastic items can be fragmented to produce secondary MNP via thermal, biological, or mechanical processes.[12]

MNP are not limited to urban environments as they have been found in uninhabited locations such as the Alps,[7] Tibetan Plateau,[8] and the Artic region.[9] These contaminants have also found their way into food sources such as rice,[11] table salt,[12] and tea[13] which could pose a hazard to consumers. Most recently, microplastics have been found in human placenta[14] and arteries.[15] In the environment, some organisms are unable to differentiate their food sources from nanoplastics,[23] resulting in the ingestion of nanoplastics that can then bioaccumulate through the food chain.[16, 17] The omnipresence of MNP has created an urgency to better understand their toxicity, fate, and impact on the environment and human health. However, to assess these factors,

we need to be able to detect, identify, and characterize these tiny particles in complex and often carbon-dominated matrices (e.g., natural waters, soils, whole organisms).

Further to this problem is the ongoing debate of the size difference between microplastics and nanoplastics. Currently, it is common to classify particles less than 1000 nm as nanoplastics,[18] 5 mm to 1000 nm as microplastics, and greater than 5 mm as macroplastics.[19] It is this definition and stipulation of size range that will be used to differentiate nanoplastics from microplastics throughout this report.

Current Detection Methodologies and their Limitations

Various tools to detect and identify MNP within complex matrices have been reported in the scientific literature. Some of the most widely used analytical tools for characterizing MNP include Raman Spectroscopy, Fourier Transform Infrared Spectroscopy (FTIR), and pyrolysis gas-chromatography-mass spectroscopy (Py-GC/MS).[20] These techniques will be discussed briefly in this section, along with a list of applications of these tools. It is important to note that many other tools aside from the ones discussed here exist with their own advantages and disadvantages. This section only serves as an overview of some of the analytical tools used in research to characterize MNP and is non-exhaustive.

FTIR

FTIR uses infrared light (primarily between 400 and 4000 cm^{-1})[21] to analyze materials. The infrared light is directed at a sample where some light is absorbed and/or transmitted. The absorbed light can cause a change in the molecules' dipole, which will transfer the vibrational energy levels from the ground state to the excited state. The interaction between IR light and the sample generates a spectrum.[22] The frequency of peaks in this spectrum is based on the difference in vibrational energy levels, whereas the intensity is based on the change of dipole moment.[23] Since each molecule will interact with the IR radiation differently, the spectrum acts as a fingerprint, unique to each molecule. This allows researchers to cross-reference the spectrum with a database, thereby identifying unknown material.

Larger microplastics are often identified using conventional FTIR. However, for chemical identification of microplastics, micro-FTIR (μ-FTIR) has been used[24]. μ-FTIR uses an optical microscope in combination with an infrared spectrometer enabling visual and chemical analysis at a higher spatial resolution[25]. A summary of some studies can be reviewed in Table 1. For example

μ-FTIR was used to identify microplastics in the drinking water supply chain in Germany[26] and to provide valuable insights on the transport of microplastics to remote regions[27].

Table 1: Overview of a few studies using FTIR for MNP detection and identification.

Authors	Method Used	MNP Type	Size	Media	Goal of Study
Julienne *et al.*[28]	μ-FTIR	PE	0.024 mm film	Air and Type 1 water	Use micro-FTIR to study weathering of PE films in air and water
Mintenig *et al.*[26]	μ-FTIR	PE, polyamide, polyester, PVC, and epoxy resin	0.050 to 0.150 mm	Ground water and drinking water	Identify microplastic throughout the drinking water supply chain in Germany
Vianello *et al.*[27]	μ-FTIR	PE, PP, polyester, PS, PVC, polyamide, alkyd resin, polyvinyl alcohol, & polyacrylonitrile	0.015 to 2.413 mm	Freshwater, seawater, and wastewater	Quantify and characterize microplastics in the Lagoon of Venice
Corami *et al.*[29]	μ-FTIR	polyester & polyamide	0 – 0.5 mm	Detergent and water (simulating household washing)	Development of a technique to characterize fibres released from household washing
Crichton *et al.*[30]	μ-ATR FTIR	PVC & PE	0.063 to 0.999 mm	Sediment samples & oil	Develop an extraction process for microplastics in aquatic sediment samples and analyzed them using FTIR
Bergmann *et al.*[31]	μ-FTIR	Varnish, rubber, PE, and polyamide	Larger than 0.011 mm	Snow	Detection of microplastics in Fram Strait and Svalbard snow samples to establish atmospheric deposition

Organic matter and other contaminants on the microplastics' surface can affect the ability of μ-FTIR to detect the sample. To overcome this challenge, researchers often resort to purification or pre-treatment of samples to remove organic matter.[21] Furthermore, μ-FTIR is limited to imaging particles larger than 20 μm.[32] This is due to the diffraction limit of the IR spectroscope, resulting

in a low spectrum intensity and quality[32]. This drawback often requires pre-screening of environmental samples, which is sometimes completed by visual inspection leading to some bias. Furthermore, Käppler *et al.* showed that FTIR identifies 35% less microplastics that are smaller than 20 μm when compared to Raman.[32] For this reason, the authors recommended using FTIR for microplastics sized between 50 to 500 μm.

Raman

Raman spectroscopy is a non-destructive characterization method that uses monochromatic light to analyze materials. When monochromatic light is directed onto the sample, scattered light is detected by the instrument. There are three types of scattering when the light interacts with the matter: Rayleigh, Stokes, and Anti-Stokes. Rayleigh scattering occurs when a molecule is excited to a virtual state and then returns to its ground state; this causes the photon to be scattered elastically. This type of scattering is the most common and has the highest intensity. Stokes scattering causes a molecule to be excited to a virtual state and return to a state with higher vibrational energy than it originally started with; this causes the photon to be scattered inelastically and have less energy than it originally started with. Lastly, Anti-Stokes scattering excites an already excited molecule to a virtual state, and then returns it to a lower vibrational energy level than it started with. This causes the photon to be scattered super elastically and have more energy than it started with. In Raman spectroscopy, Stokes scattering is used to measure the photon's change in energy, measured as a frequency change.[33]

Like FTIR, Raman spectroscopy is often used for microplastic and nanoplastic research, as seen by some studies listed in Table 2. For example, Allen *et al.* used Raman to understand the atmospheric transport of microplastics in the French Pyrenees,[34] and Zhang *et al.* combined Raman with scanning electron microscopy (SEM) to identify nanoplastics from recycled PVC[35] and were able to identify particles as small as 360 nm. Overall, Raman spectroscopy is often used for particles smaller than 20 μm and is less constrained in terms of the thickness of the sample and interferences from glass, CO_2, and water.[36] Raman spectroscopy enables visualization of particles as small as 1 micron due to the smaller wavelength of light used[37]. This is evident by the Abbe's equation which states decreasing imaging wavelength will increase spatial resolution. Some studies have optimized Raman signal intensity to detect 100 nm nanoplastics. Overall, Raman

spectroscopy is advantageous as it provides an image of the sample, which can help identify the shape and size of the particle, which is in addition to identifying the chemical composition.[32]

Table 2: Overview of a few studies using Raman for MNP detection and identification.

Authors	Method Used	MNP Type	Size	Media	Goal of Study
Gündoğdu[12]	Micro-Raman	PE & PP	20 µm to 5 mm	Table salt	Study the concentration and identification of microplastics in 16 table salt brands in Turkey
Allen *et al.*[34]	Micro-Raman	PS, PE, PP, & PVC	50 to 300 µm	Atmospheric wet and dry deposition	Study the transport of microplastics to remote uninhabited areas
Xiong *et al.*[38]	Micro-Raman	PE & PP	0.1 to 0.5 mm	Lake surface water, river water, & lakeshore sediment	Identify and detect microplastic pollution in China's freshwater systems
Sobhani *et al.*[39]	Micro-Raman	PS & polyacrylic paint particles	100 nm to 600 nm	Type 1 water	Characterize nanoplastics using micro-Raman mapping and validation using generated paint particles
Zhang *et al.*[35]	Raman + SEM	Recycled PVC powders	360 - 1920 nm	Type 1 water	Identify and analyze the shape of nanoplastic powder from recycled PVC

Although Raman is an excellent tool for submicron particle identification, it becomes less reliable when fluorescent emissions or dyes are present in the sample.[21] Degradation of the sample under Raman spectroscopy has also been reported due to the use of a laser light.[40] This is caused when the laser results in plasmonic heating, where the temperature of the particle can increase past the glass transition temperature, resulting in physical changes in the polymer.[41]

Since FTIR and Raman are common tools in microplastic analysis, studies using and comparing the two instruments are prevalent in literature, as seen in Table 3. For example, Cabernard *et al.* compared Raman with FTIR by analyzing microplastics in surface water.[42] The authors concluded that micro-Raman could identify 23% more microplastics than ATR-FTIR. However, the analysis time for Raman is significantly higher than that of FTIR; the authors stated

it took 147 hours per 100 L of water examined. As a consequence, the authors discuss the need to develop a more efficient methodology for micro-Raman. Although micro-Raman was more successful in identifying microplastics than ATR-FTIR in this study, the authors admit that more than 66% of particles were unidentifiable due to the organic and biological contaminants in their environmental samples.

Table 3: Overview of a few studies using FTIR and Raman for MNP detection and identification.

Authors	**Method Used**	**MNP Type**	**Size**	**Media**	**Goal of Study**
Käppler *et al.*[32]	FTIR and Raman	PE, PS, PAN	1 µm to 5 mm	Sediment	Compared Raman and FTIR to analyze environmental samples
Wagner *et al.*[43]	FTIR and Raman	PE & PP	100 to 600 µm	Digestive tract of fish	Study microplastic extraction after pre-treatment in lab cultivated fish and ocean surface fish samples
Lares *et al.*[44]	FTIR and Raman	PET	0.5 to 1 mm	Municipal wastewater	Evaluate WWTP's efficiency in removing microplastic using optical microscopy, FTIR, Raman
Cabernard *et al.*[42]	FTIR and Raman	PE, PP, PS, and PMMA	10 µm to 5 mm	Surface water	Compare Raman's and FTIR's ability to quantify microplastics from environmental aquatic samples

Py-GC/MS

Py-GC/MS thermally degrades the sample, releasing gasses that are then analyzed through gas chromatography and mass spectroscopy, where chemical composition can be identified. This allows for not only the identification of the MNP but also the various additives in the sample, which is one of the main advantages of this tool. A few examples in literature include the use of Py-GC/MS to identify nanoplastics in river, sea, and influent/effluent water samples from a wastewater treatment plant;[45] drinking water and surface water from a freshwater system;[46] sand water extracts;[47] and soil matrices;[48] as seen in Table 4.

Table 4: Overview of a few studies using Py-GC/MS for MNP detection and identification.

Authors	Method	MNP Type	Size	Media	Goal of Study
Yanagisawa *et al.*[49]	Py-TD-GC/MS	Polyethylene terephthalate (PET), Acrylonitrile butadiene styrene (ABS), PVC, PS	Not reported	Various organic solvents	Identify additives in polymers by creating reference material for the Py-GC/MS
Herrera *et al.*[50]	Double shot Py/GC-MS	ABS (virgin and recycled)	Not reported	N/A	Develop a fast method to identify the additives from electronic plastic waste
Dekiff *et al.*[51]	Py-GC/MS	PE, PP, PS, Polyamide (PA), PVC, PET	0.1 to 1 mm	Sediments from Island of Norderney	Study spatial distribution of microplastics on beach sediments
Funck *et al.*[52]	Py-GC/MS	PS and PE	10 µm and larger	WWTP effluent	Apply a cascade filtering method to separate microplastics of different sizes and identify the polymer and additive type
Dierkes *et al.*[53]	Py-GC/MS	PE, PS	10 to 400 µm	Sediments from River Rhine	Develop a method using pressurized liquid extraction to quantify microplastics
Dessì *et al.*[11]	Double shot Py/GC-MS	PE, PET, PMMA, PP, PS, PVC	Not reported	Rice	Study the concentration of plastics present in various rice from grocery stores in Australia
Elert *et al.*[54]	Raman, FTIR, and TED-GC/MC	PE, PP, PS, PET	150 to 200 µm	Soil	Compare three microplastic characterization methods

Fischer and Scholz-Böttcher[55]	Curie-Point Py-GC/MS	PE, PVC, PS, PET, PMMA, PA	Not reported	Fish	Develop methodology to quantify and identify microplastics using thermochemolysis and Py-GC/MS
Käppler *et al.*[56]	FTIR and Py-GC/MS	PE, PP, PS, PVC, PET, polyvinyl alcohol, ethylene vinyl acetate, PTFE	500 µm to 5 mm	Sediments from Warnow River	Compare FTIR's and Py-GC/MS's ability to identify microplastics
Ribeiro *et al.*[57]	Py-GC/MS + µFTIR	PE, PP, PVC, PS, PMMA	1 to 2236 µm	Oysters	A combined approach to characterize plastics and understand the size distribution in oysters

However, this identification method is destructive[58] and therefore samples cannot be reused for further analysis. Particles cannot be localized in a sample (e.g., whole organism) because the entire sample is destroyed during analysis. Furthermore, information about individual MNP cannot be retrieved, such as size and morphology.[36] Py-GC/MS is also sensitive/dependent on the mass of the microplastic. Käppler *et al.* compared Py-GC/MS and µ-ATR-FTIR to identify microplastics and fibres from sediment samples.[56] From the 27 particles sampled, three of them could not be identified by Py-GC/MS because of the low particle mass. The authors also noted that Py-GC/MS measurement time was significantly longer than FTIR, stating a factor of 30 to 100 in terms of length. Overall, the instrument's destructive nature is a major disadvantage; as a result, a better methodology for detecting and identifying nanoplastics must be established.

Hyperspectral Imaging

More recently, hyperspectral imaging (HSI) has been employed for the detection and identification of MNP. This method is label-free, preserves spatial information, and detects nanoplastics. In general, HSI uses visible light or near infrared light to acquire a spectrum for every pixel from a sample image. This spectrum can be used to match an unknown spectrum to a known spectrum thereby enabling the detection of unidentified samples. A major limitation of using HSI is its low resolution resulting in identification of particles that are 100 microns or larger.[59] One recommendation to overcome the lower resolution is to combine HSI with another imaging

technique, such as stereomicroscopes.[59] An example of this would be the enhanced darkfield hyperspectral imaging (EDF-HSI), which uses darkfield microscopy in conjunction with HSI, providing both spatial and hyperspectral information. In general, EDF-HSI uses a halogen bulb as its light source and then directs the light through a condenser at the base of the microscope.[60] The directed light path results in a high signal-to-noise ratio, enabling a resolution of 2 nm. A darkfield stop is used to generate a darkfield image where the sample is illuminated, leaving the background dark. The oblique light rays' interactions with the sample scatters the light, which enters the objective lens. The light is then directed to the CCD camera and spectrometer from the objective lens. The spectrometer generates the spectral information of the sample, known as a hyperspectral data cube. From this, the spectrum of any pixel from an image can be retrieved. Furthermore, by creating a reference library containing the spectra of a known material, the identification of an unknown sample is possible. Processing software (e.g., ENVI in the CytoViva) can cross-reference the spectra of an unknown sample with the reference library. Table 5 shows some recent studies using EDF-HSI for MNP detection. It is important to note that studies using EDF-HSI were the focus of the brief literature search as this technique enables detection of nanoplastics whereas HSI is limited by its resolution.

Table 5: Overview of a few studies using HSI for MNP detection and identification

Authors	**Method**	**MNP Type**	**Size**	**Media**	**Goal of Study**
Ishmukhametov *et al.*[61]	EDF-HSI and deep learning	PS	1 µm	human skin fibroblasts	To combine machine learning and EDF-HSI to detect microplastics within biological samples.
Nigamatzyanova and Fakhrullin[62]	EDF-HSI	PS and PMMA	100 nm, 200 nm, 500 nm, 1 µm	*Caenorhabditis elegans* (*C. elegans*)	Detect ingested microplastic within a model organism
Fournier *et al.*[63]	EDF-HSI	PS	20 nm	rat fetal tissues	Translocation of nanoplastics from maternal to fetal
Rahman *et al.*[64]	EDF-HSI	PS, LDPE, PP, polyamid	various sizes	air sampling	Optimize collection and characterization of environmental MNP samples

		e-nylon powder, and environmentally collected MNP			

Although EDF-HSI enables detection of nanoplastics and uses a label-free method, interference of biomass is still of concern when using non-translucent organisms. Furthermore, some studies listed in Table 5 employ pre-labelled, fluorescent, or coloured particles. Although coloured particles are representative of environmental MNP, pre-labelled and fluorescent particles are limited to controlled experiments and generally irrelevant to the analysis of environmental samples.

Research Gaps

It is evident that there are many studies that are successful in detecting and identifying microplastics within complex matrices. However, the small size of nanoplastics makes it difficult for conventional and vibrational microscope techniques to detect these particles. Hence, there is a need to develop methods that can detect nanoplastics, especially when the smaller nanoplastics are more harmful than microplastics.[65] To further understand MNP toxicity, detecting ingested MNP within organisms without losing spatial information is essential. This requires the analysis of non-translucent organisms and pre-treatment that preserves organism morphology.

Many studies also use pre-labelled particles for toxicity studies. This limits toxicologists to particles that are not necessarily representative of environmental MNP. Furthermore, there is concern that pre-labelled particles have some toxicity compared to pristine unlabelled plastic particles due to dye leaching.[66] Therefore, another research gap exists in this area, where a label-free method to detect ingested MNP needs to be developed.

Particle concentrations used in many studies are not representative of environmental conditions with studies using concentrations up to seven orders of magnitude higher than what is found in the environment.[67] This disconnect can lead to misrepresentation of MNP toxicity on organisms. A review article by Shen *et al.* concluded that many studies used environmentally irrelevant concentrations; as a result, they urged future studies to focus on lower and more environmentally relevant concentrations of MNP to gauge their environmental impacts.[68]

Thesis Objectives

In an effort to address the knowledge gaps identified above, this study proposes the combination of histology techniques with enhanced dark field hyperspectral imaging (EDF-HSI), where histology is the process of taking thin micron sized slices of a sample embedded in paraffin or frozen media. This method enables researchers to see within a biological sample without altering its morphology. In this study, cryotomy will be used to acquire histological slices. Additionally, hematoxylin and eosin (H&E) staining will be applied to differentiate biomass from plastic. This is to take advantage of the unique capabilities of the EDF-HSI microscope that allows for hyperspectral analysis for the detection of MNP. Overall, the following objectives will be assessed in this study:

1. To determine if the combination of histology and EDF-HSI enables the detection of MNP within whole organisms
2. To determine if H&E staining alters the spectrum of biomass to enable detection of nanoplastics within whole organisms
3. To determine if the proposed method is applicable to different plastic types
4. To determine if the proposed method is applicable to environmentally relevant nanoplastic concentrations

This thesis is presented in a manuscript-based format as per "McGill Guidelines for Thesis Preparation". Chapter 2 presents an original research manuscript which includes details about the methodology, results, and discussions. The conclusion and future work are discussed in Chapter 3.

Chapter 2: Detection of Microplastics and Nanoplastics within a Whole Organism using Hyperspectral Imaging and Histology

Introduction

Plastic pollution has become ubiquitous and is an emerging contaminant in aquatic and terrestrial environments. Large plastic waste breaks down into smaller microplastics (1 μm to 5 mm)[19] and nanoplastics (smaller than 1000 nm)[18] (MNP) due to weathering conditions such as, UV irradiation, mechanical degradation, biological degradation, and temperature fluctuations. MNP have been found in the most remote locations, such as high-altitude Alps[7] and Tibetan Plateau,[8] with the potential of microplastics to be transported to the Arctic region.[9] These contaminants have also been detected in various foods and beverages such as rice,[11] table salt,[12] beer,[69] tea,[13] and wine,[70] exposing consumers to MNP. In the environment, some organisms are unable to differentiate their food sources from nanoplastics.[71] This results in the ingestion of nanoplastics that can then bioaccumulate through the food chain, where humans stand at the apex. Most recently, microplastics have been found in the human placenta[14] and arteries.[15] The omnipresence of MNP has created an urgency to better understand their toxicity, fate, and impacts on the environment and human health. However, to assess these factors, there is a need for adequate methods to detect, identify, and characterize these tiny particles. More importantly, detecting ingested MNP within whole organisms will enable localization within certain organs or tissues thereby improving our understanding of their toxicity, such as changes to hormones, morphology, behaviour, and reproduction. Therefore, there is an increased importance and need for the development of methodologies that enables detection of MNP within whole organisms.

The novelty of these contaminants has motivated the development of various tools to detect and identify MNP within complex matrices. Mass spectroscopy techniques identify MNP and their additives but lose spatial information.[72] Vibrational techniques, such as Raman and FTIR, are the most commonly used analytical tools for identifying microplastics within a sample.[32, 42] However, FTIR is often limited to identifying microplastics larger than 20 microns, and the presence of organic components can interfere with obtaining accurate results for both Raman and FTIR.[72] For nanoplastics, electron microscopy techniques have been used to characterize these smaller particles. However, careful sample preparation is required, including coating the sample with a conductive material.[73] Most analytical techniques used for detecting and identifying MNP within

biological samples also require extensive pre-treatment, such as digestions to remove organic matter that can interfere and hinder with spectrum acquisition.[20] This can involve the use of harmful solvents that can melt,[74] decompose,[75] or discolour[76] plastic present in the sample.

An alternative to pre-treatment of samples by digestion is the use of dyes to differentiate between the biological sample and the particles. For example, fluorescent dyes are often applied to particles prior to organism exposure, resulting in the organism of interest ingesting pre-dyed particles.[77] This method allows the use of a wide range of plastic particles that can be prepared and dyed in the laboratory or purchased from a commercial supplier, thereby providing crucial ecotoxicity information on a broader range of plastic types. However, these commercially available fluorescent particles' size, shape, and surface properties are not always environmentally relevant. Furthermore, dyes can leach out of the particles, resulting in the misidentification of particles.[78] The leached dye may also pose some toxicity to the organism, making it difficult to determine if organism toxicity is due to the dye or the plastic particle.[66] Another example of dye application is costaining, which involves applying two dyes simultaneously, where one acts as a counter stain. For example, Nile red, in conjunction with 4′,6-Diamidino-2-phenylindole (DAPI), has been used where Nile red binds with plastic particles, and DAPI binds only with biological material.[78] However, there is still concern over dye specificity and, thereby, uncertain detection of particles. Hence, there is a need to develop a label-free method that enables detection of MNP within biological samples.

Hyperspectral imaging (HSI) is a label-free, non-destructive, and rapid method that has been used for the detection and identification of microplastics. In general, HSI uses visible or near infrared light to acquire a spectrum for every pixel from a sample image. The combination of acquiring spatial information and spectral data makes it an advantageous tool for particle characterization. For example, HSI has been used to characterize microplastics collected in the Po River, Italy,[79] as well as spiked microplastics within intestinal tracts of fish,[80] digested mussel tissue,[81] and farmland soil samples.[82] However, due to the lower resolution of traditional HSI, it can only characterize microplastics greater than 100 microns,[59] with most papers studying particles larger than 300 microns. For smaller particles, enhanced darkfield hyperspectral imaging (EDF-HSI) has been proposed due to its higher signal-to-noise ratio.[60] In fact, EDF-HSI has been used for the detection of silver nanoparticles (>10 nm) in water samples,[83, 84] polymer-coated Au/CuS nanoparticles (>25 nm) human cells,[85] and gold nanoparticles (>15 nm) in *Daphnia magna.*[86] EDF-

HSI has also been used to detect MNP in matrices such as human cells[61] and *C. elegans.*[62] However, the presence of biomass in a sample can interfere with the acquisition of the spectral signal used to identify MNP. This study proposes the combination of histology techniques with EDF-HSI to enable improved visualization inside the organism when non-translucent organisms are studied. Also, to overcome the issue of biomass interference with the HSI detection, hematoxylin and eosin (H&E) staining will be applied to the whole organism after MNP exposure to enable the differentiation of biomass from plastic. H&E staining is selective to biomass, ensuring the internalized plastic remains primarily unstained. This, therefore, changes the spectra of biomass compared to the plastic, enabling hyperspectral analysis to locate and detect plastic particles within the whole organism.

Methods

Daphnia magna Exposure

Daphnia magna (D. magna) was chosen as the model organism as it is commonly used in MNP ecotoxicological studies.[87] Environment and Climate Change Canada (SPE1/RM/14, 2000) guidelines were followed for maintaining the *D. magna* culture. *D. magna* were cultured in moderately hard reconstituted water (comprising 60 mg/L $MgSO_4$, 96 mg/L $NaHCO_3$, 4 mg/L KCl, 60 mg/L $CaSO_4 \cdot 2H_2O$, 2 mg/L Na_2SeO_4, and 2 mg/mL vitamin B12 in deionized water) in glass beakers. The beakers were kept in a controlled incubator (Panasonic, MLR-352) at 20 °C for 48 h with a 16/8 h day/night cycle. The culture was fed with cultured green algae (*Chlorella vulgaris)* and yeast-cerophyl-trout mix (Arofish, USA).

Adult *D. magna* (7 days old) were exposed to 0.1 ppm and 0.01 ppm of 750 nm, 500 nm, unlabeled polystyrene (PS) beads (Polysciences 07309-5 and 09836-5) under acute toxicity conditions (48-hour exposure). *D. magna* were also exposed to 20 ppm of polyethylene (PE) particles with a size distribution of 200 nm to 9900 nm (Cospheric 140411-1). Here, the 500 nm PS at 0.01 ppm serves as the environmentally relevant treatment condition.[88] Each of the following treatments 500 nm PS at 0.01 ppm, 750 nm PS at 0.1 ppm, and 20 ppm of PE particles, were separately suspended in moderately hard reconstituted water. The treatments' suspension volume was 40 mL in 50 mL glass beakers, with five adult *D. magna* in each beaker. The beakers were kept in a temperature-controlled incubator (Panasonic, MLR-352) at 20 °C for 48 h with a 16/8 h

day/night cycle for the duration of their exposure. After exposure, *D. magna* were preserved in Bouin's solution (Sigma Aldrich HT10132) for at least 24 h where the samples perished.

Cryotome Slices

After at least 24 h of preservation in Bouin's solution, adult *D. magna* were rinsed with a phosphate buffered solution (VWR E404), then embedded in Optimal Cutting Temperature resin (Sakura 4583) and frozen in liquid nitrogen. A cryotome (Leica 3050s) was then used to obtain histological sections of the *D. magna*. The cryotome was thoroughly cleaned using acetone prior to sectioning. The chamber and sample holder temperatures were set to –25 ºC. Each histological slice was 20 µm thick, and *D. magna* were sliced on the transverse plane. Samples were collected on positively charged glass slides (Fisher Scientific 1255015), where each histological slice flash-dried onto the slides.

Staining

Prior to staining, histological slices on glass slides were rinsed with deionized (DI) water to remove the resin. Histological slices on glass slides were rehydrated by submerging the samples in decreasing ethanol concentrations (100%, 75%, 50% and then DI water) for 1 minute per concentration. Next, hematoxylin (Sigma-Aldrich HHS32) and eosin (Sigma-Aldrich R030340-74) were used to stain the histological slices. Various concentrations of equal parts of hematoxylin and eosin (H&E) stain in DI water were tested to establish the optimal concentration. H&E stain was applied at concentrations of 100%, 50%, 25%, 10%, and 5% v/v. The staining protocol was adapted from Feldman and Wolfe.[89] First, the slides were submerged in hematoxylin for at least 30 seconds. Following that, the slides were rinsed in DI water. Next, the slides were stained with eosin for at least 90 seconds. Immediately after staining was completed, samples were rehydrated by submerging the samples in decreasing ethanol concentrations (100%, 75%, 50% and then DI water) for at least 1 minute per concentration. Staining and rehydration were completed at room temperature. Histological slices were imaged in darkfield mode on a stereomicroscope (Olympus SZX16) before and after staining.

Imaging and Analysis on Enhanced Darkfield Hyperspectral Imaging Microscope

Next, the slides were imaged using enhanced darkfield hyperspectral imaging (EDF-HSI). The EDF-HSI microscope is fitted with an Olympus BX41 upright microscope, CytoViva® high-

aperture dark-field condenser (CytoViva Inc., USA), and CytoViva® 10×, 60×, and 100× objective lens. A halogen bulb (International Light Technologies L1090) was used as the light source. Spectral information was captured using a spectrophotometer (CytoViva Hyperspectral Imaging System, Auburn, AL.). ENVI 4.8 software was used to capture images at an exposure time of 250 ms using 696 lines, providing a full field of view. Spectra were captured in the visual near-infrared region of 400 nm to 1000 nm at a 2 nm resolution using a spectrograph. This data (spatial information in the x-y plane and hyperspectral data in the z-plane) is stored in a hypercube in the ENVI 4.8 software. Prior to imaging, all slides were fitted with a glass cover slip with one drop of Type 1 immersion oil.

Two reference libraries were created containing the spectra of pristine polystyrene (PS) and polyethylene (PE) particles suspended in DI water. In Figure S1, reference PS and PE particles and their corresponding average spectrum can be observed. The reference libraries were created by using the Region of Interest tool to obtain the spectra of 30-35 pixels. The spectrum of the chosen pixels was saved as the reference library, which was then used to detect PS and PE within the sample images using the Spectral Angle Mapping (SAM) tool. A matching angle of 0.085 radians was used. Figure 1 shows an overview of the methodological workflow.

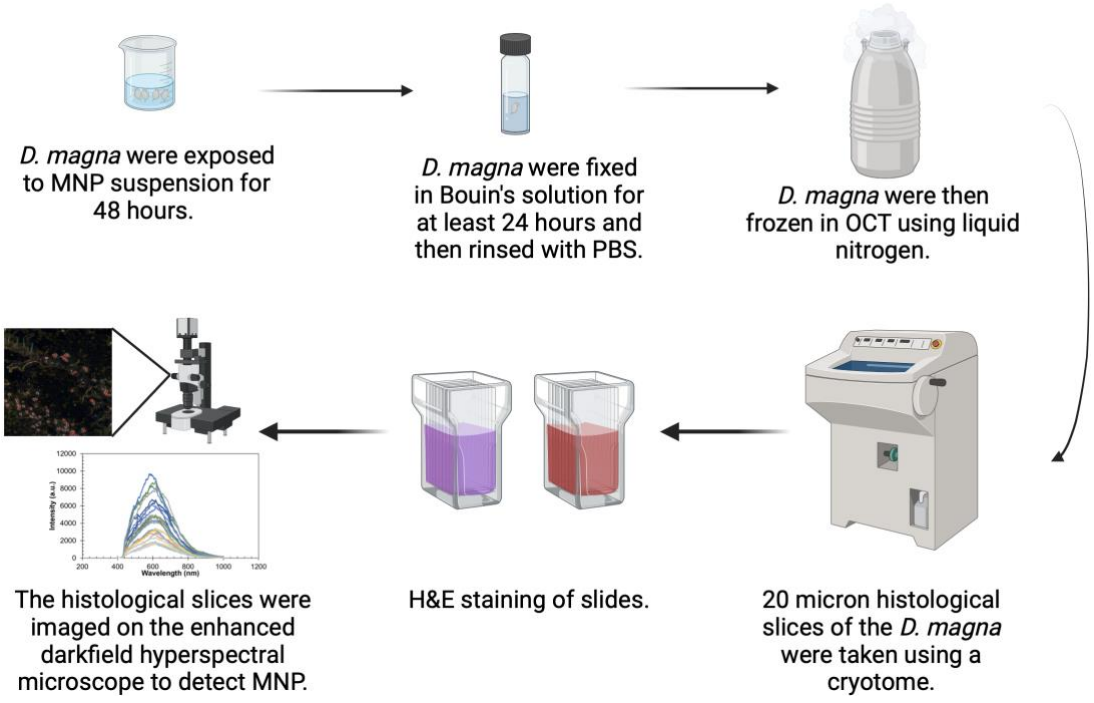

Figure 1. Schematic of the overall procedure to obtain histological slices, subsequent H&E staining, and image acquisition. Figure was created with BioRender.com

Results and Discussion

Carbon-based material, such as organic matter and biomass, often hinders the detection of MNP in environmental samples and organisms. Cryotome techniques can be used to reduce the interference from the tissue and biomass when analyzing the uptake of MNP while preserving the organism's structure. Thus, the first objective of this study was to show that cryotome techniques, when combined with EDF-HSI, enable visualization of nanoplastics within a whole organism. In Figure 2A, a sample image of *D. magna* can be observed prior to obtaining histological slices.

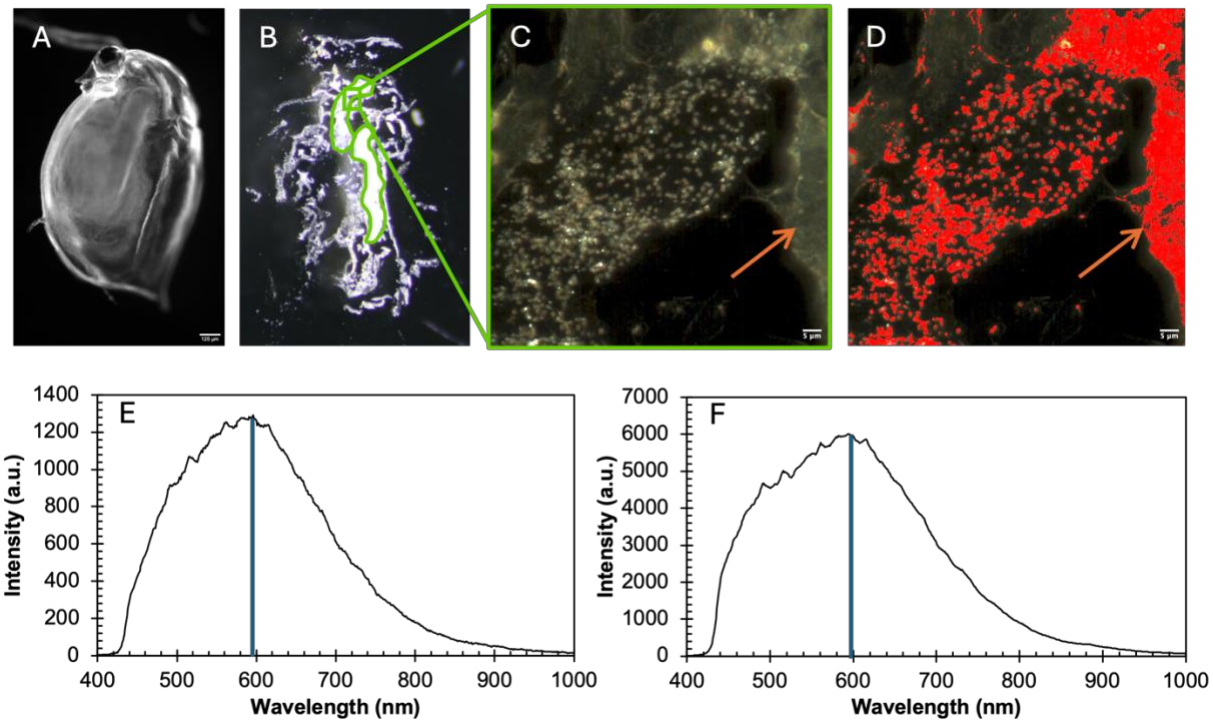

Figure 2. Detection of MNP within a whole organism. Fig. 2A depicts a darkfield image of *D. magna* acquired on an optical microscope. Fig. 2B is a 20 µm thick histological slice of a *D. magna* exposed to 750 nm PS at a concentration of 0.1 ppm. The gut region of the *D. magna* is outlined in green. Fig. 2C is a darkfield image acquired on the EDF-HSI microscope. This image is taken in the gut region as shown by the green box. The orange arrow points to an area where only biomass is present. Fig. 2D shows the Spectral Angle Mapping of the darkfield image taken in Fig. 2C. Areas in red indicate where the spectra matched the reference spectra for PS. Fig. 2E is the average spectra of 50 pixels of biomass from Fig. 2C. The peak wavelength is 596 nm, as shown by the blue line. Fig. 2F is the average spectra of 50 pixels of 750 nm PS from Figure S2A. The peak wavelength is 594 nm, as shown by the blue line.

In Figure 2B, the gut region of *D. magna* can be identified on the histological slice. Next, EDF-HSI was used to acquire images to visualize the ingested nanoplastic, as seen in Figure 2C. The smaller nanoplastic fraction is more challenging to detect with common analytical techniques due to the diffraction limit of light. However, EDF-HSI's high signal-to-noise ratio enables the detection of some nanoparticles as small as 10 nm.[83] In Figure S1, a darkfield image acquired on the EDF-HSI microscope provides the reference size and shape of pristine PS and PE particles. Using the ENVI software, Spectral Angle Mapping tool was used which matches the spectra of every pixel from the sample image with the spectra in the reference library of PS. The red regions in Figure 2D represent the pixels where the measured spectra matched the reference spectra for PS. Here, the plastic particles are detected; however, some of the biomass (shown with the orange arrow in Figure 2C and D) was also mislabelled as plastic. As shown in Figure 2E-F, the spectra for PS and biomass exhibit similar signatures in terms of shape and peak maxima. This similarity can lead to the Spectral Angle Mapping tool to misinterpret biomass as plastic particles. One strategy to overcome this issue is to stain the organism with the aim of modifying the biomass spectral response but leaving the spectra of the particles mostly unchanged. As such, an H&E staining protocol was implemented to effectively differentiate biomass from plastics.

Hematoxylin stains nuclei and tissue, whereas eosin acts as a counterstain, staining cytoplasmic compounds. H&E staining is commonly used for histopathology.[89, 90] Due to H&E's selective staining, it was used to stain the biomass on the histological slice. A similar technique has also been employed in other studies using ATR-FTIR[91] and light microscopy.[92, 93] In this work, the H&E staining is applied after cryotome samples have been collected to create a post-exposure staining process, enabling the use of label-free particles during the organism exposure phase.

To optimize the staining procedure using H&E to enhance Spectral Angle Mapping, different ratios of the stain were studied. Concentrations of each respective stain in DI water were tested at 5%, 10%, 25%, 50% and 100% (v/v) as presented in Figure 3. After applying the Spectral Angle Mapping tool to detect nanoplastics, parts of the biomass are misidentified as plastic when 5% and 10% v/v H&E stains are used. It is evident that staining results in a change to the spectrum's shape and peak wavelength. However, the change in the spectrum's shape is significantly less pronounced for 5% and 10%, indicating that 5% and 10% staining is inadequate in differentiating biomass spectra from plastic. This is further supported by the spectra shown in Figure 3M, where 5% and 10% staining result in smaller red shift (0% peak wavelength 597 nm;

5% peak wavelength 616 nm, 10% peak wavelength 639 nm). In addition to red shifting of the biomass' spectrum for 25%, 50%, and 100% concentrations (peak wavelengths 656 nm, 685 nm, and 659 nm respectively), their spectrum shape has also significantly changed where two peaks can be observed compared to the single peak for 0%, 5%, and 10% staining. Since 25% v/v H&E results in adequate changes to the spectrum compared to the control (0% stain) while using minimum stain, it was chosen as the optimal concentration to use for the remainder of the study.

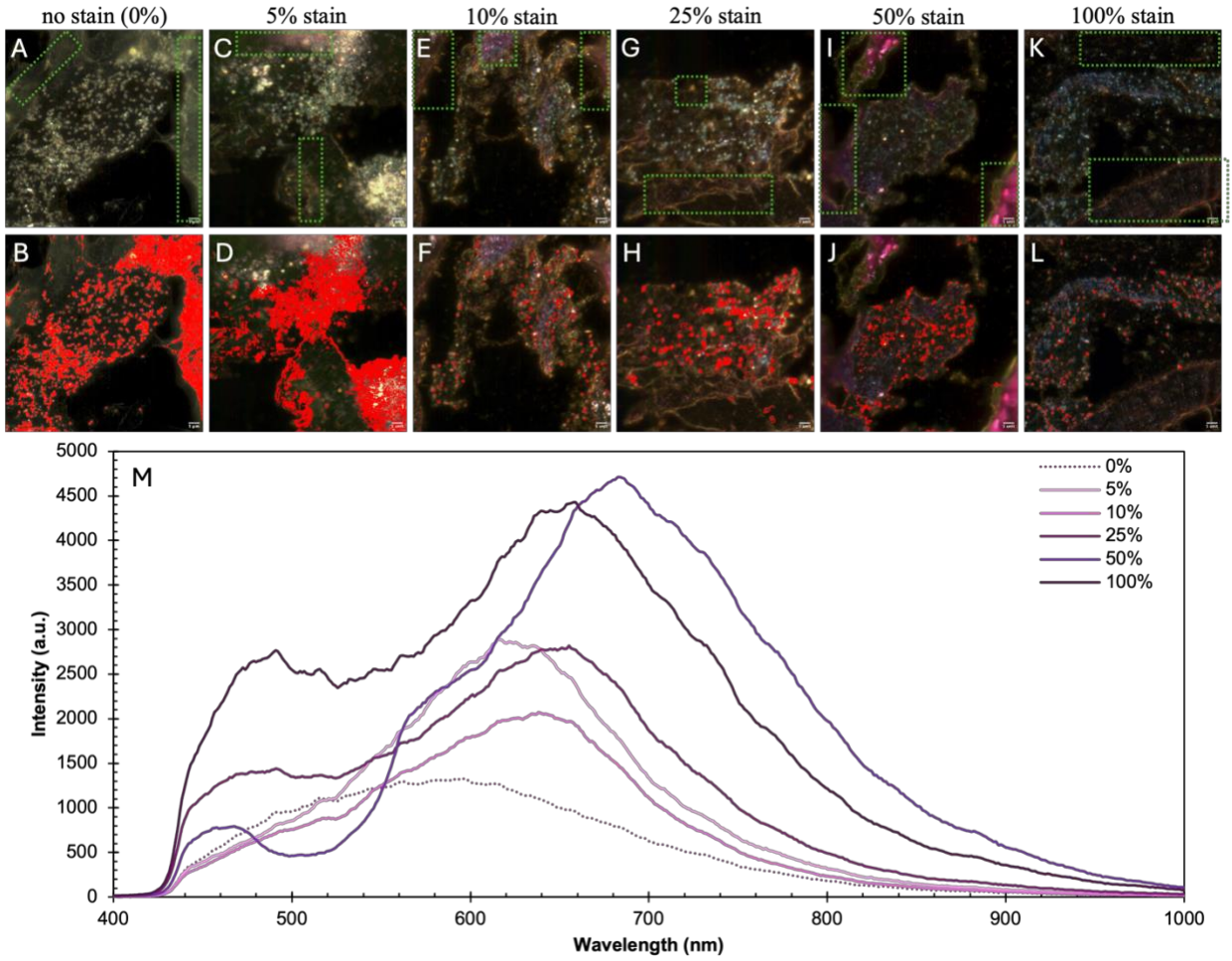

Figure 3. H&E staining of histological slices at different stain concentrations. All *D. magna* were exposed to 750 nm PS at a concentration of 0.1 ppm, and all histological slices were 20 µm thick. Fig. 3A is unstained, and the corresponding Spectral Angle Mapping image is in Fig. 3B, where red parts indicate mapped areas (i.e., matches with the PS library). The remaining panels show images of *D. magna* stained with different concentrations of stain: Fig. 3C-D have been stained with 5% H&E, Fig. 3E-F have been stained with 10% H&E, Fig. 3G-H have been stained with 25% H&E, Fig .3I-J have been stained with 50% H&E, and Fig. 3K-L have been stained

with 100% H&E. Fig. 3D, F, H, J, and L are the Spectral Angle Mapping images where red parts indicate mapped areas. Fig. 3M is the average spectra of 50 pixels of biomass from each of the histological slices from Fig. 3A, C, E, G, I, and K. Green boxes on Fig. 3A, C, E, G, I, and K indicate the regions where the biomass spectra for each staining concentration were measured.

To confirm that H&E staining at a concentration of 25% v/v does not label the plastic, PS and PE particles were exposed to the staining protocol and mapped using their respective reference library. Visual inspection of Figure S2 and Figure S3 indicates that 25% v/v H&E staining does not stain PS and PE. The shape of the plastic spectrum remains unchanged before and after staining. Furthermore, the peak wavelength of unstained PE was 596 nm, and after staining the peak wavelength was 592 nm. Likewise, peak wavelength of unstained PS was 616 nm, and after staining the peak wavelength was 615 nm. This is supported by the accurate mapping of PE and PS particles using Spectral Angle Mapping tool in Figure S2 and Figure S3.

Overall, 25% (v/v) H&E staining was mainly selective to the biomass, thereby altering the spectra of the biomass but leaving the spectra of the PS and PE mostly unchanged (Figure 3M). The peak wavelength of biomass before staining was 597 nm, and after staining the biomass peak wavelength has red shifted to 656 nm. The resulting red shift in the spectra allows for the differentiation between plastic particles and the biomass. When Spectral Angle Mapping is applied to the stained histological slices, the average spectra of the nanoplastic observed in the histological slice match with the average spectra of pristine PS plastic (Figure S4), suggesting that the spherical particles are PS. Furthermore, three histological slices of a *D. magna* control sample, which was not exposed to MNP, was also analyzed to ensure the Spectral Angle Mapping tool does not identify any biomass as PS after staining, as shown in Figure S5.

Vertical Image Stacks

Due to the 20 μm thick histological slices, some areas of acquired darkfield images were more in-focus than other parts, as evident in Figure 4A, where particles that are in focus are identified with a green arrow. The remaining particles can still be visually observed but are distorted due to the scattering of light. This results in the Spectral Angle Mapping tool to identify more areas as plastic, evident in Figure 4D. To address this, images were acquired throughout the histological slice's z-axis, essentially creating a vertical stack of images, shown in Figure 4A-C. Acquiring images at various focal depths is helpful in visually confirming particles that are present

in those areas. Figure 4B and C confirm that the Spectral Angle Mapping algorithm correctly detected nanoplastics; the green arrows in Figure 4B and C point to particles that were not in focus on Figure 4A. Additional examples of vertical stacks can be observed in Figure S7 and S8.

One study had expressed concern that particles were shifting or dislodging from the sample when obtaining histological slices.[94] Aramendia *et al.* suggested that the observation of particles embedded within the biomass confirms the localization of particles in an area.[95] Similarly, in this study, nanoplastics were observed at various focal depths in the histological slice. This suggests that the detected nanoplastics are, in fact, localized in the gut rather than transported or dislodged during slicing by the blade.

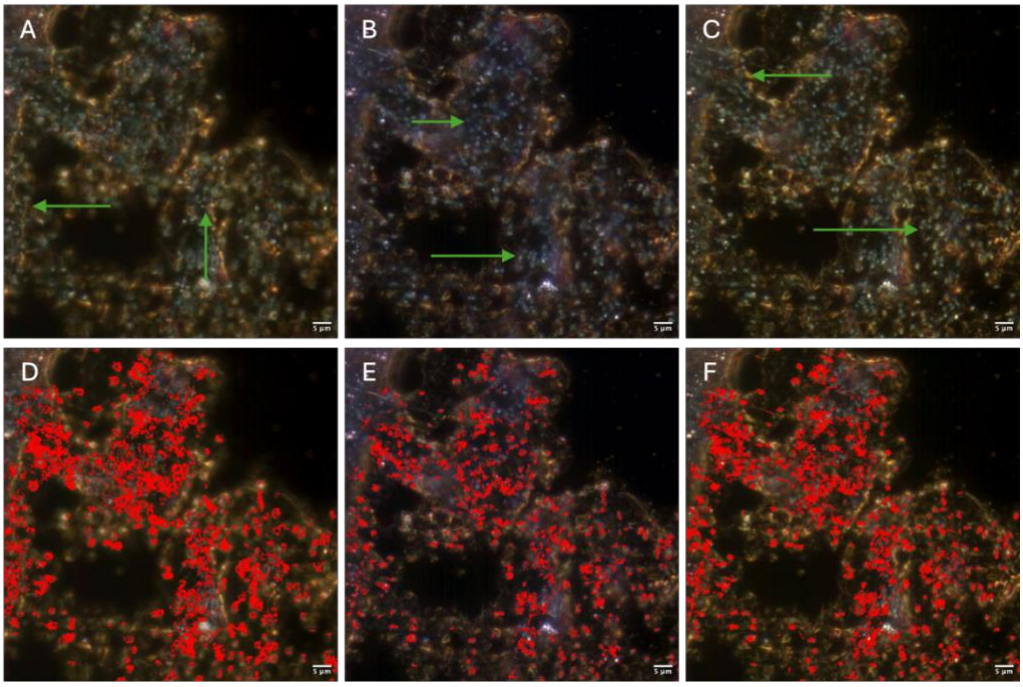

Figure 4: Vertical-stack of *D. magna* exposed to 750 nm PS particles at a concentration of 0.1 ppm. Histological slices were stained with 25% H&E staining. Fig. 4A is the first image in the vertical stack where the green arrows point towards to a few particles that are in focus compared to the other particles. Fig. 4D is the corresponding Spectral Angle Mapping image where red parts indicate the detection of the PS particles. Fig. 4B is the second image in the stack, where the distorted particles from Fig. 4A are in focus, shown by the green arrows. Fig. 4E is the corresponding Spectral Angle Mapping image where red parts indicate the detection of the PS particles. Fig. 4C is the last image in the vertical stack, where new particles in focus are shown

with a green arrow. Fig. 4F is the corresponding Spectral Angle Mapping image where red parts indicate the detection of the PS particles.

Another alternative to ensure detection of all particles in a slice is to use thinner histological slices. For example, 10 µm slices will cause less interference from the biomass. A drawback with the thinner slices is that the *D. magna* structure may not be conserved as well. Hence, researchers intending to use this method to detect plastic particles within their sample can use thinner histological slices, such as 10 µm, at the expense of losing some spatial integrity of the organism and possibly disturbing the localization of particles within the organism. This will allow for an improved mapping of particles in the sample, and therefore, potentially detection of particles. However, if researchers are more interested in the spatial distribution of particles within the organism, then 20 µm thick histological slices should be used at the expense of quantification of particles in the biomass.

Applicability of Method to Different Plastic Types, Sizes, and Concentrations

The new protocol was applied to PE particles with a size distribution between 200 nm to 9900 nm at 20 ppm. Since PE floats when suspended in water, this affects the actual exposure dose. Thus, a higher exposure concentration was used here to increase the probability of *D. magna* ingesting the particles. This is evident in Figure 5, where only a few particles are observed on the histological slice of *D. magna* exposed to PE. In Figure 5, PE particles can visually be seen within the gut region of *D. magna* and detected by the Spectral Angle Mapping tool.

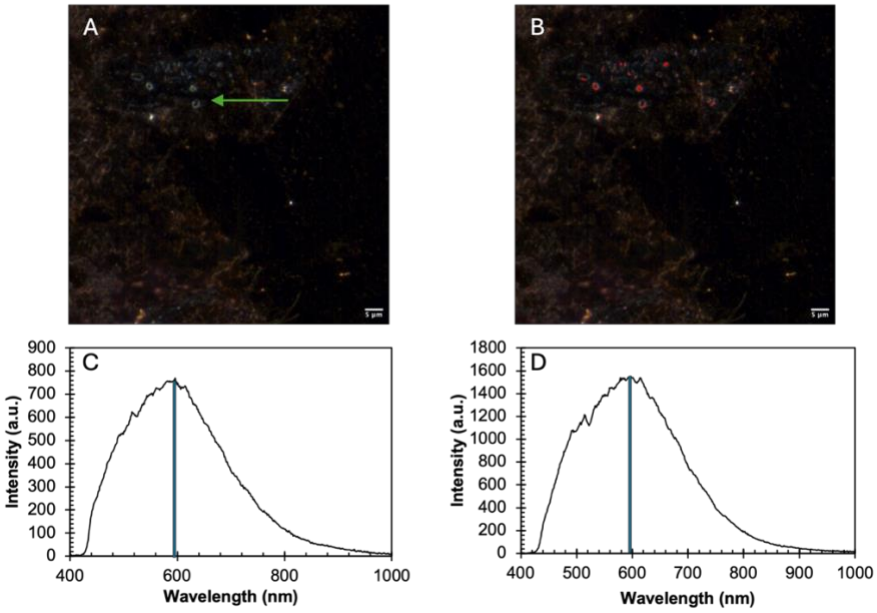

Figure 5. Detection of PE nanoplastics within the gut region of *D. magna*. Histological slices were stained with 25% H&E staining. Fig. 5A is a darkfield image of the gut region where a PE particle is shown with a green arrow. Fig. 5B is the corresponding Spectral Angle Mapping image where PE particles are detected shown by the red areas. Fig. 5C is the average spectrum of reference PE particles where the peak wavelength is 596 nm. Fig 5D is the average spectrum of PE particles detected in the darkfield image where the peak wavelength is 594 nm.

To further test the limits of this method, smaller-sized nanoplastics and lower-concentration exposures were completed. Figure 6 represents a histological slice of *D. magna* exposed to 500 nm particles at a concentration of 0.01 ppm. For reference, 500 nm PS particles suspended in DI water can be observed in Figure S1. Although it is difficult to visually observe 500 nm particles within the histological slice, Spectral Angle Mapping enables the detection of the smaller nanoplastic within a sample using the proposed methodology. With the resolution of the EDF-HSI microscope enabling visualization of particles as small as 100 nm,[62] the method proposed in this study theoretically can detect particles smaller than 500 nm. However, further work must be carried out to detect nanoplastics smaller than 500 nm within whole organisms. Another example of detection of 500 nm PS at a concentration of 0.01 ppm can be observed in Figure S9.

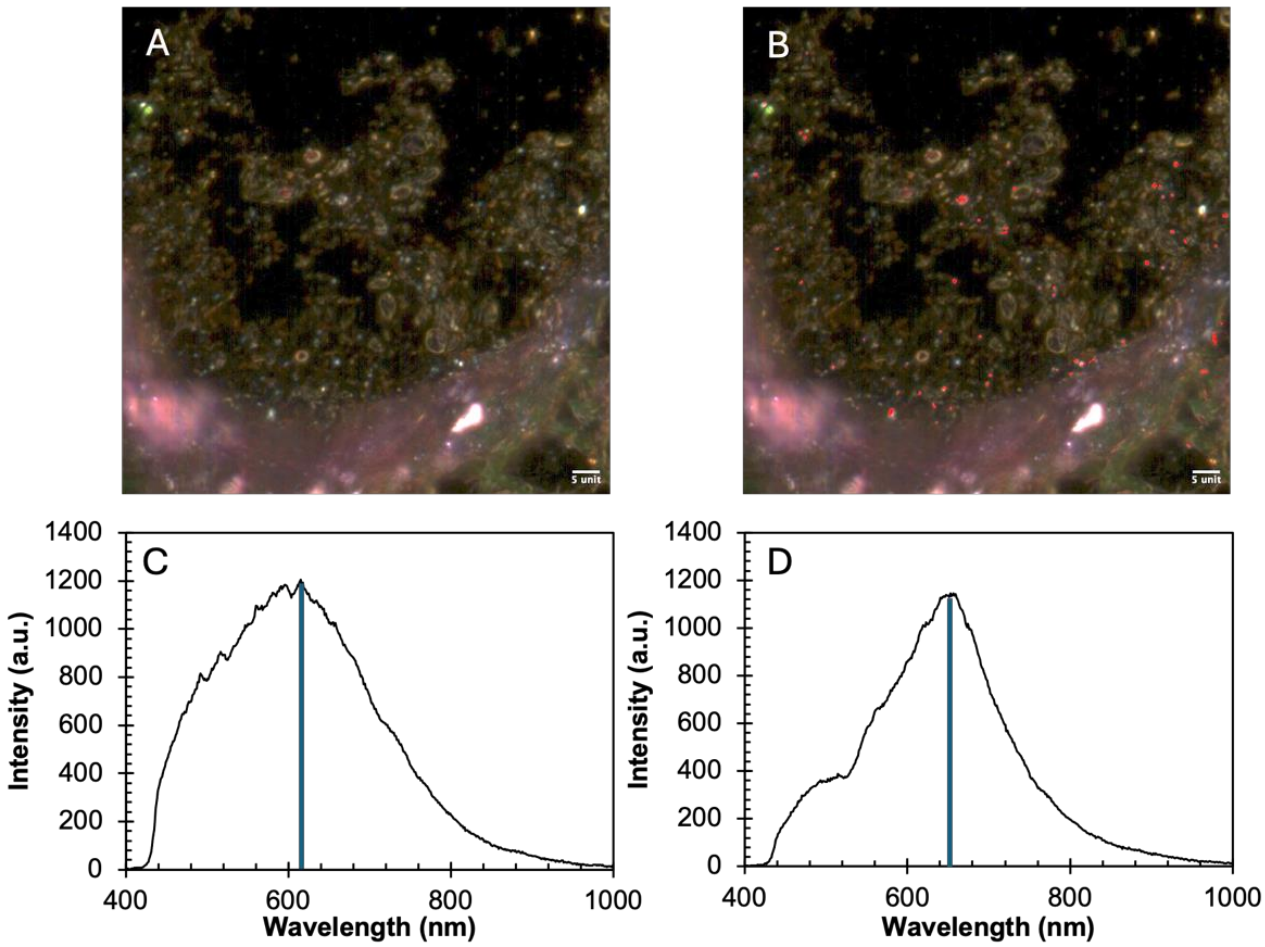

Figure 6. Detection of ingested 500 nm PS at a concentration 0.01 ppm in *D. magna*. Histological slices were stained with 25% H&E staining. Fig. 6A is the darkfield image acquired on the EDF-HSI microscope of a 20 µm thick histological slice of *D. magna* exposed to 500 nm PS at a concentration of 0.01 ppm. Fig. 6B is the corresponding Spectral Angle Mapping image which shows the detection of PS particles in red. Fig. 6C is the average spectra of 50 pixels of plastic particles from Fig 6A. The peak wavelength of 615 nm is shown with the blue line. Fig. 6D is the average spectra of 50 pixels of biomass from Fig. 6A. The peak wavelength of 652 nm is shown with the blue line.

The detection of MNP at low concentrations, such as 0.01 ppm, enables researchers to implement lower concentrations in controlled ecotoxicology experiments. This will provide new insights into the toxicology of these emerging contaminants. Furthermore, the ability to detect MNP at lower concentrations is more relevant to environmental conditions, as shown by Shi *et al.* who found nanoplastic concentrations in freshwater environments range from 0.0003 to 0.433 ppm

[88]. Thus, this method may be useful to determine the presence of MNP at low concentrations in freshwater samples.

Limitations and Future Work

One of the limitations of the new method is the inability of the Spectral Angle Mapping tool to differentiate between plastic types. Since hyperspectral data acquired from this method uses a halogen light source emitting visible light, two pixels with a similar RGB profile will result in a similar spectrum. Hence, plastic particles that are similar in colour cannot be differentiated. Figure S4 shows the average spectra of some plastic types, where all of the spectra are similar in shape and peak wavelengths (PS – 594 nm, PE – 596 nm, and PTFE – 561 nm). This indicates the challenge of identifying the plastic type using the EDF-HSI technique alone, thereby requiring additional techniques for the identification of the plastic. Combining this technique with optical photothermal infrared microscopy (O-PTIR) enables the detection and identification of MNP. A combination of different imaging techniques can lead to more accurate MNP detection methods[59, 113] and future work will focus on creating a methodology using EDF-HSI and O-PTIR.

In this study, pristine MNP were used. However, it is also important to study MNP that are relevant to environmental samples. Hence, future studies will explore whether the proposed methodology can be applied using weathered MNP as well as environmental samples. Preliminary results of weathering of 3 μm PS microplastic for 45 days indicates the spectrum after weathering does not change, as shown in Figure S10. After using the Spectral Angle Mapping tool, all particles were detected using the reference library of pristine PS particles. Hence, it is hypothesized that this methodology can be useful to detect weathered MNP within whole organisms.

Conclusion

The detection of nanoplastics has been challenging and one of the limiting factors in improving our understanding of their fate and impacts in the environment. This work proposes a method to detect MNP within a whole organism using hyperspectral imaging and histological techniques. Hematoxylin and eosin stains are used to selectively label biomass, thereby changing its spectral signature. This allows for spectral angle mapping to be carried out, enabling detection of nanoplastics within a histological slice, while preserving spatial distribution. Although the instrument cannot identify which type of plastic is present within the sample, this method proves to be an efficient procedure to quickly detect nanoplastics as small as 500 nm at environmentally

relevant concentrations. Furthermore, this post-exposure labeling methodology can be especially useful for toxicology studies, eliminating the need to use pre-labelled plastic particles.

Acknowledgements and Funding:

This project was funded by McGill University through the McGill Engineering Eugenie Ulmer Lamothe Scholarship, the Natural Sciences and Engineering Research Council of Canada (NSERC) through its Pollution in Urban Environments Collaborative Research and Training Experience (PURE CREATE) program and Discovery program, Fonds de Recherche Nature et technologies through its EcotoQ program and Team Projects program, the Canada Research Chairs program, Fisheries and Oceans Canada (DFO), and the Canada Foundation for Innovation.

Chapter 3: Conclusions and Future Work

The omnipresence of MNP has urged scientists to better understand their impact on the environment and human health. However, effective methodologies to detect and identify these small, emerging contaminants in complex carbon-rich matrices need to be developed. More precisely, detection of MNP within whole organisms is a challenging task. Yet, it would provide invaluable information such as localization of particles in organs and their respective toxicity. This study aimed to address this challenge by developing a label-free methodology to detect MNP within whole organisms.

The combination of histological techniques and EDF-HSI microscopy enabled the detection of MNP within the model organism, *D. magna*. EDF-HSI microscopy provides a high signal-to-noise ratio, enabling the detection of nanoplastics, which are often difficult to capture due to the diffraction limit of light. The instrument's capability to provide spatial and hyperspectral information makes it a valuable tool for MNP detection in complex matrixes. Histology techniques, such as cryotomy, enables spectral acquisition of MNP with minimum biomass hinderance.

Using a post exposure staining process with H&E stains, biomass was selectively stained thereby differentiating the spectra of biomass and MNP within each histological slice. The peak wavelength of unstained biomass was 597 nm, whereas stained biomass' peak wavelength red shifted to 656 nm. 750 nm PS particles' peak wavelength after staining was 615 nm. The difference between the stained biomass spectra and PS particles allowed for the detection of MNP using the Spectral Angle Mapping algorithm. Furthermore, the staining process was optimized by selecting a concentration of H&E stain that adequately changed the spectra of biomass while minimizing the amount of stain used. The optimal stain concentration of 25% v/v was selected.

In addition to the detection of 750 nm PS nanoplastics, smaller-sized particles at lower concentrations of 0.01 ppm were also identified within a whole organism. Furthermore, this study presented the application of the methodology on other plastic types, such as PE microplastics, which were also detected using the SAM tool. Thereby confirming that H&E stains were selective towards biomass, and not plastic.

The results of this study indicate that the detection of label-free MNP within a whole organism at very low concentrations is possible. More importantly, the use of a post-exposure

labelling process allows for the use of non-commercial and label-free particles to be used. This can also include environmentally collected MNP samples, providing direct information of the toxic impact of MNP from the environment on organisms. Theoretically, organisms collected from the environment can also be analyzed for any ingested MNP, providing information on the fate of MNP. Overall, the proposed methodology provides an additional tool for researchers to use for the detection of MNP, thereby increasing our knowledge and understanding of these emerging contaminants.

The advantages of this methodology include the detection of nanoplastics within organisms, the detection of nanoplastics in low concentrations, and the applicability to different plastic types. However, the inability to identify the type of plastic within the sample is a limitation of this method. This can be overcome by combining additional imaging tools such as, optical photothermal infrared imaging (O-PTIR). O-PTIR is a novel instrument that acquires both IR and Raman spectra of a sample. This enables chemical identification of the polymer type. Furthermore, the use of visible light to thermally expand the sample enables acquisition of IR spectra and detection of nanoplastic as small as 500 nm.

Furthermore, the instrument's ability to detect MNP is limited by the reference library, especially in the case of environmental MNP samples. Therefore, it is recommended to create larger reference libraries containing various types of pristine, lab-weathered, and environmentally weathered plastics. Moreover, creating open-access libraries can not only improve the reference library's database but also allow anyone to use the library. Nonetheless, the presented method can still detect the presence of nanoplastics quickly within a sample and be used as an initial screening for plastic particles.

Future work to address the limitations of this method can include using O-PTIR to confirm the identity of the plastic, and further validate the findings of this study. Furthermore, it is important to note that MNP found in the environment are exposed to weathering conditions which alter their chemical and physical properties. Weathered MNP are a more significant threat than pristine plastics and require more research to understand their impact and fate on the environment. Hence, future work will focus on using weathered MNP to see if the same methodology can be applied. Preliminary results, presented in Figure S10, indicate the spectra of weathered MNP does not significantly shift, which does not affect detection using the Spectral Angle Mapping tool. A reference library will also be created based on the weathered MNP to improve detection of those

types of plastics. Lastly, many studies, such as the one presented here, focus on aquatic organisms, yet terrestrial organisms are rarely studied. Future work on exploring the application of this method should also use terrestrial organisms such as *Drosophila melanogaster*.

This study presented a method that is non-destructive and label-free which allows for subsequent analysis using other characterization techniques. Overall, combining histology with EDF-HSI and staining protocols has enabled the detection of nanoscale particles within whole organisms. Although the present study has its own limitation and future work is required, it does provide an additional method for the detection of MNP.

References

(1) Geyer, R. Chapter 2 - Production, use, and fate of synthetic polymers. In *Plastic Waste and Recycling*, Letcher, T. M. Ed.; Academic Press, 2020; pp 13-32.

(2) Zalasiewicz, J.; Waters, C. N.; Ivar do Sul, J. A.; Corcoran, P. L.; Barnosky, A. D.; Cearreta, A.; Edgeworth, M.; Gałuszka, A.; Jeandel, C.; Leinfelder, R.; et al. The geological cycle of plastics and their use as a stratigraphic indicator of the Anthropocene. *Anthropocene* **2016**, *13*, 4-17. DOI: https://doi.org/10.1016/j.ancene.2016.01.002.

(3) Crutzen, P. J. The "Anthropocene". In *Earth System Science in the Anthropocene*, Ehlers, E., Krafft, T. Eds.; Springer Berlin Heidelberg, 2006; pp 13-18.

(4) Geyer, R.; Jambeck, J. R.; Law, K. L. Production, use, and fate of all plastics ever made. *Science Advances* **2017**, *3* (7), e1700782. DOI: doi:10.1126/sciadv.1700782.

(5) Jambeck, J. R.; Geyer, R.; Wilcox, C.; Siegler, T. R.; Perryman, M.; Andrady, A.; Narayan, R.; Law, K. L. Plastic waste inputs from land into the ocean. *Science* **2015**, *347* (6223), 768-771.

(6) Ritchie, H.; Roser, M. Plastic Pollution. *Our World in Data* **2018**. (acccessed November 8, 2022).

(7) Materić, D.; Ludewig, E.; Brunner, D.; Röckmann, T.; Holzinger, R. Nanoplastics transport to the remote, high-altitude Alps. *Environmental Pollution* **2021**, *288*, 117697. DOI: https://doi.org/10.1016/j.envpol.2021.117697.

(8) Zhang, Y.; Gao, T.; Kang, S.; Allen, S.; Luo, X.; Allen, D. Microplastics in glaciers of the Tibetan Plateau: Evidence for the long-range transport of microplastics. *Science of The Total Environment* **2021**, *758*, 143634. DOI: https://doi.org/10.1016/j.scitotenv.2020.143634.

(9) Evangeliou, N.; Grythe, H.; Klimont, Z.; Heyes, C.; Eckhardt, S.; Lopez-Aparicio, S.; Stohl, A. Atmospheric transport is a major pathway of microplastics to remote regions. *Nature Communications* **2020**, *11* (1), 3381. DOI: 10.1038/s41467-020-17201-9.

(10) PlasticsEurope, E. *Plastics—The Facts 2022*. 2022. https://plasticseurope.org/wp-content/uploads/2022/10/PE-PLASTICS-THE-FACTS_V7-Tue_19-10-1.pdf (accessed 2022 November 1).

(11) Dessì, C.; Okoffo, E. D.; O'Brien, J. W.; Gallen, M.; Samanipour, S.; Kaserzon, S.; Rauert, C.; Wang, X.; Thomas, K. V. Plastics contamination of store-bought rice. *Journal of Hazardous Materials* **2021**, *416*, 125778. DOI: https://doi.org/10.1016/j.jhazmat.2021.125778.

(12) Gündoğdu, S. Contamination of table salts from Turkey with microplastics. *Food Additives & Contaminants: Part A* **2018**, *35* (5), 1006-1014. DOI: 10.1080/19440049.2018.1447694.

(13) Hernandez, L. M.; Xu, E. G.; Larsson, H. C.; Tahara, R.; Maisuria, V. B.; Tufenkji, N. Plastic teabags release billions of microparticles and nanoparticles into tea. *Environmental science & technology* **2019**, *53* (21), 12300-12310.

(14) Garcia, M. A.; Liu, R.; Nihart, A.; El Hayek, E.; Castillo, E.; Barrozo, E. R.; Suter, M. A.; Bleske, B.; Scott, J.; Forsythe, K.; et al. Quantitation and identification of microplastics accumulation in human placental specimens using pyrolysis gas chromatography mass spectrometry. *Toxicological Sciences* **2024**, *199* (1), 81-88. DOI: 10.1093/toxsci/kfae021 (acccessed 6/30/2024).

(15) Marfella, R.; Prattichizzo, F.; Sardu, C.; Fulgenzi, G.; Graciotti, L.; Spadoni, T.; D'Onofrio, N.; Scisciola, L.; La Grotta, R.; Frigé, C. Microplastics and nanoplastics in atheromas and cardiovascular events. *New England Journal of Medicine* **2024**, *390* (10), 900-910.

(16) Habumugisha, T.; Zhang, Z.; Fang, C.; Yan, C.; Zhang, X. Uptake, bioaccumulation, biodistribution and depuration of polystyrene nanoplastics in zebrafish (Danio rerio). *Science of The Total Environment* **2023**, *893*, 164840. DOI: https://doi.org/10.1016/j.scitotenv.2023.164840.

(17) Mattsson, K.; Ekvall, M. T.; Hansson, L.-A.; Linse, S.; Malmendal, A.; Cedervall, T. Altered Behavior, Physiology, and Metabolism in Fish Exposed to Polystyrene Nanoparticles. *Environmental Science & Technology* **2015**, *49* (1), 553-561. DOI: 10.1021/es5053655.

(18) Gigault, J.; Halle, A. t.; Baudrimont, M.; Pascal, P.-Y.; Gauffre, F.; Phi, T.-L.; El Hadri, H.; Grassl, B.; Reynaud, S. Current opinion: What is a nanoplastic? *Environmental Pollution* **2018**, *235*, 1030-1034. DOI: https://doi.org/10.1016/j.envpol.2018.01.024.

(19) Frias, J. P. G. L.; Nash, R. Microplastics: Finding a consensus on the definition. *Marine Pollution Bulletin* **2019**, *138*, 145-147. DOI: https://doi.org/10.1016/j.marpolbul.2018.11.022.

(20) Nguyen, B.; Claveau-Mallet, D.; Hernandez, L. M.; Xu, E. G.; Farner, J. M.; Tufenkji, N. Separation and Analysis of Microplastics and Nanoplastics in Complex Environmental Samples. *Accounts of Chemical Research* **2019**, *52* (4), 858-866. DOI: 10.1021/acs.accounts.8b00602.

(21) Caldwell, J.; Taladriz-Blanco, P.; Lehner, R.; Lubskyy, A.; Ortuso, R. D.; Rothen-Rutishauser, B.; Petri-Fink, A. The micro-, submicron-, and nanoplastic hunt: A review of detection methods for plastic particles. *Chemosphere* **2022**, *293*, 133514. DOI: https://doi.org/10.1016/j.chemosphere.2022.133514.

(22) Nicolet, T. *Introduction to Fourier Transform Infrared Spectrometry*. Thermo Nicolet Corporation, 2001. https://www.chem.uci.edu/~dmitryf/manuals/Fundamentals/FTIR%20principles.pdf (accessed November 26, 2022).

(23) Birkner, N.; Wang, Q. *How an FTIR Spectrometer Operates*. LibreTexts, 2022. https://chem.libretexts.org/@go/page/1844 (accessed November 26, 2022).

(24) Shim, W. J.; Hong, S. H.; Eo, S. E. Identification methods in microplastic analysis: a review. *Analytical Methods* **2017**, *9* (9), 1384-1391, 10.1039/C6AY02558G. DOI: 10.1039/C6AY02558G.

(25) Chen, Y.; Zou, C.; Mastalerz, M.; Hu, S.; Gasaway, C.; Tao, X. Applications of Micro-Fourier Transform Infrared Spectroscopy (FTIR) in the Geological Sciences--A Review. *Int J Mol Sci* **2015**, *16* (12), 30223-30250. DOI: 10.3390/ijms161226227 From NLM.

(26) Mintenig, S. M.; Löder, M. G. J.; Primpke, S.; Gerdts, G. Low numbers of microplastics detected in drinking water from ground water sources. *Science of The Total Environment* **2019**, *648*, 631-635. DOI: https://doi.org/10.1016/j.scitotenv.2018.08.178.

(27) Vianello, A.; Boldrin, A.; Guerriero, P.; Moschino, V.; Rella, R.; Sturaro, A.; Da Ros, L. Microplastic particles in sediments of Lagoon of Venice, Italy: First observations on occurrence, spatial patterns and identification. *Estuarine, Coastal and Shelf Science* **2013**, *130*, 54-61. DOI: https://doi.org/10.1016/j.ecss.2013.03.022.

(28) Julienne, F.; Delorme, N.; Lagarde, F. From macroplastics to microplastics: Role of water in the fragmentation of polyethylene. *Chemosphere* **2019**, *236*, 124409. DOI: https://doi.org/10.1016/j.chemosphere.2019.124409.

(29) Corami, F.; Rosso, B.; Bravo, B.; Gambaro, A.; Barbante, C. A novel method for purification, quantitative analysis and characterization of microplastic fibers using Micro-FTIR. *Chemosphere* **2020**, *238*, 124564. DOI: https://doi.org/10.1016/j.chemosphere.2019.124564.

(30) Crichton, E. M.; Noël, M.; Gies, E. A.; Ross, P. S. A novel, density-independent and FTIR-compatible approach for the rapid extraction of microplastics from aquatic sediments. *Analytical Methods* **2017**, *9* (9), 1419-1428, 10.1039/C6AY02733D. DOI: 10.1039/C6AY02733D.

(31) Bergmann, M.; Mützel, S.; Primpke, S.; Tekman, M. B.; Trachsel, J.; Gerdts, G. White and wonderful? Microplastics prevail in snow from the Alps to the Arctic. *Science Advances* **2019**, *5* (8), eaax1157. DOI: doi:10.1126/sciadv.aax1157.

(32) Käppler, A.; Fischer, D.; Oberbeckmann, S.; Schernewski, G.; Labrenz, M.; Eichhorn, K.-J.; Voit, B. Analysis of environmental microplastics by vibrational microspectroscopy: FTIR, Raman or both? *Analytical and Bioanalytical Chemistry* **2016**, *408* (29), 8377-8391. DOI: 10.1007/s00216-016-9956-3.

(33) Raja, P. M. V.; Barron, A. R. Raman Spectroscopy. (acccessed December 4, 2022).

(34) Allen, S.; Allen, D.; Phoenix, V. R.; Le Roux, G.; Durántez Jiménez, P.; Simonneau, A.; Binet, S.; Galop, D. Atmospheric transport and deposition of microplastics in a remote mountain catchment. *Nature Geoscience* **2019**, *12* (5), 339-344. DOI: 10.1038/s41561-019-0335-5.

(35) Zhang, W.; Dong, Z.; Zhu, L.; Hou, Y.; Qiu, Y. Direct Observation of the Release of Nanoplastics from Commercially Recycled Plastics with Correlative Raman Imaging and Scanning Electron Microscopy. *ACS Nano* **2020**, *14* (7), 7920-7926. DOI: 10.1021/acsnano.0c02878.

(36) Jakubowicz, I.; Enebro, J.; Yarahmadi, N. Challenges in the search for nanoplastics in the environment—A critical review from the polymer science perspective. *Polymer Testing* **2021**, *93*, 106953. DOI: https://doi.org/10.1016/j.polymertesting.2020.106953.

(37) Sobhani, Z.; Al Amin, M.; Naidu, R.; Megharaj, M.; Fang, C. Identification and visualisation of microplastics by Raman mapping. *Analytica Chimica Acta* **2019**, *1077*, 191-199. DOI: https://doi.org/10.1016/j.aca.2019.05.021.

(38) Xiong, X.; Zhang, K.; Chen, X.; Shi, H.; Luo, Z.; Wu, C. Sources and distribution of microplastics in China's largest inland lake – Qinghai Lake. *Environmental Pollution* **2018**, *235*, 899-906. DOI: https://doi.org/10.1016/j.envpol.2017.12.081.

(39) Sobhani, Z.; Zhang, X.; Gibson, C.; Naidu, R.; Megharaj, M.; Fang, C. Identification and visualisation of microplastics/nanoplastics by Raman imaging (i): Down to 100 nm. *Water Research* **2020**, *174*, 115658. DOI: https://doi.org/10.1016/j.watres.2020.115658.

(40) Araujo, C. F.; Nolasco, M. M.; Ribeiro, A. M. P.; Ribeiro-Claro, P. J. A. Identification of microplastics using Raman spectroscopy: Latest developments and future prospects. *Water Research* **2018**, *142*, 426-440. DOI: https://doi.org/10.1016/j.watres.2018.05.060.

(41) Mogha, N. K.; Shin, D. Nanoplastic detection with surface enhanced Raman spectroscopy: Present and future. *TrAC Trends in Analytical Chemistry* **2023**, *158*, 116885. DOI: https://doi.org/10.1016/j.trac.2022.116885.

(42) Cabernard, L.; Roscher, L.; Lorenz, C.; Gerdts, G.; Primpke, S. Comparison of Raman and Fourier Transform Infrared Spectroscopy for the Quantification of Microplastics in the Aquatic Environment. *Environmental Science & Technology* **2018**, *52* (22), 13279-13288. DOI: 10.1021/acs.est.8b03438.

(43) Wagner, J.; Wang, Z.-M.; Ghosal, S.; Rochman, C.; Gassel, M.; Wall, S. Novel method for the extraction and identification of microplastics in ocean trawl and fish gut matrices. *Analytical Methods* **2017**, *9* (9), 1479-1490, 10.1039/C6AY02396G. DOI: 10.1039/C6AY02396G.

(44) Lares, M.; Ncibi, M. C.; Sillanpää, M.; Sillanpää, M. Occurrence, identification and removal of microplastic particles and fibers in conventional activated sludge process and advanced MBR technology. *Water Research* **2018**, *133*, 236-246. DOI: https://doi.org/10.1016/j.watres.2018.01.049.

(45) Zhou, X.-x.; Hao, L.-t.; Wang, H.-y.-z.; Li, Y.-j.; Liu, J.-f. Cloud-Point Extraction Combined with Thermal Degradation for Nanoplastic Analysis Using Pyrolysis Gas Chromatography–Mass Spectrometry. *Analytical Chemistry* **2019**, *91* (3), 1785-1790. DOI: 10.1021/acs.analchem.8b04729.

(46) Mintenig, S.; Bäuerlein, P. S.; Koelmans, A. A.; Dekker, S. C.; Van Wezel, A. Closing the gap between small and smaller: towards a framework to analyse nano-and microplastics in aqueous environmental samples. *Environmental Science: Nano* **2018**, *5* (7), 1640-1649.

(47) Davranche, M.; Lory, C.; Juge, C. L.; Blancho, F.; Dia, A.; Grassl, B.; El Hadri, H.; Pascal, P.-Y.; Gigault, J. Nanoplastics on the coast exposed to the North Atlantic Gyre: Evidence and traceability. *NanoImpact* **2020**, *20*, 100262. DOI: https://doi.org/10.1016/j.impact.2020.100262.

(48) Wahl, A.; Le Juge, C.; Davranche, M.; El Hadri, H.; Grassl, B.; Reynaud, S.; Gigault, J. Nanoplastic occurrence in a soil amended with plastic debris. *Chemosphere* **2021**, *262*, 127784. DOI: https://doi.org/10.1016/j.chemosphere.2020.127784.

(49) Yanagisawa, H.; Maruyama, F.; Fujimaki, S. Verification of simultaneous screening for major restricted additives in polymer materials using pyrolyzer/thermal desorption gas–chromatography mass spectrometry (Py/TD-GC-MS). *Journal of Analytical and Applied Pyrolysis* **2019**, *137*, 37-42. DOI: https://doi.org/10.1016/j.jaap.2018.11.004.

(50) Herrera, M.; Matuschek, G.; Kettrup, A. Fast identification of polymer additives by pyrolysis-gas chromatography/mass spectrometry. *Journal of Analytical and Applied Pyrolysis* **2003**, *70* (1), 35-42. DOI: https://doi.org/10.1016/S0165-2370(02)00078-5.

(51) Dekiff, J. H.; Remy, D.; Klasmeier, J.; Fries, E. Occurrence and spatial distribution of microplastics in sediments from Norderney. *Environmental Pollution* **2014**, *186*, 248-256. DOI: https://doi.org/10.1016/j.envpol.2013.11.019.

(52) Funck, M.; Yildirim, A.; Nickel, C.; Schram, J.; Schmidt, T. C.; Tuerk, J. Identification of microplastics in wastewater after cascade filtration using Pyrolysis-GC–MS. *MethodsX* **2020**, *7*, 100778. DOI: https://doi.org/10.1016/j.mex.2019.100778.

(53) Dierkes, G.; Lauschke, T.; Becher, S.; Schumacher, H.; Földi, C.; Ternes, T. Quantification of microplastics in environmental samples via pressurized liquid extraction and pyrolysis-gas chromatography. *Analytical and Bioanalytical Chemistry* **2019**, *411* (26), 6959-6968. DOI: 10.1007/s00216-019-02066-9.

(54) Elert, A. M.; Becker, R.; Duemichen, E.; Eisentraut, P.; Falkenhagen, J.; Sturm, H.; Braun, U. Comparison of different methods for MP detection: What can we learn from them, and why asking the right question before measurements matters? *Environmental Pollution* **2017**, *231*, 1256-1264. DOI: https://doi.org/10.1016/j.envpol.2017.08.074.

(55) Fischer, M.; Scholz-Böttcher, B. M. Simultaneous Trace Identification and Quantification of Common Types of Microplastics in Environmental Samples by Pyrolysis-Gas Chromatography–Mass Spectrometry. *Environmental Science & Technology* **2017**, *51* (9), 5052-5060. DOI: 10.1021/acs.est.6b06362.

(56) Käppler, A.; Fischer, M.; Scholz-Böttcher, B. M.; Oberbeckmann, S.; Labrenz, M.; Fischer, D.; Eichhorn, K.-J.; Voit, B. Comparison of μ-ATR-FTIR spectroscopy and py-GCMS as identification tools for microplastic particles and fibers isolated from river sediments. *Analytical and Bioanalytical Chemistry* **2018**, *410* (21), 5313-5327. DOI: 10.1007/s00216-018-1185-5.

(57) Ribeiro, F.; Okoffo, E. D.; O'Brien, J. W.; O'Brien, S.; Harris, J. M.; Samanipour, S.; Kaserzon, S.; Mueller, J. F.; Galloway, T.; Thomas, K. V. Out of sight but not out of mind: Size

fractionation of plastics bioaccumulated by field deployed oysters. *Journal of Hazardous Materials Letters* **2021**, *2*, 100021. DOI: https://doi.org/10.1016/j.hazl.2021.100021.

(58) Strungaru, S.-A.; Jijie, R.; Nicoara, M.; Plavan, G.; Faggio, C. Micro- (nano) plastics in freshwater ecosystems: Abundance, toxicological impact and quantification methodology. *TrAC Trends in Analytical Chemistry* **2019**, *110*, 116-128. DOI: https://doi.org/10.1016/j.trac.2018.10.025.

(59) Faltynkova, A.; Johnsen, G.; Wagner, M. Hyperspectral imaging as an emerging tool to analyze microplastics: A systematic review and recommendations for future development. *Microplastics and Nanoplastics* **2021**, *1* (1), 13. DOI: 10.1186/s43591-021-00014-y.

(60) Fakhrullin, R.; Nigamatzyanova, L.; Fakhrullina, G. Dark-field/hyperspectral microscopy for detecting nanoscale particles in environmental nanotoxicology research. *Science of The Total Environment* **2021**, *772*, 145478. DOI: https://doi.org/10.1016/j.scitotenv.2021.145478.

(61) Ishmukhametov, I.; Nigamatzyanova, L.; Fakhrullina, G.; Fakhrullin, R. Label-free identification of microplastics in human cells: dark-field microscopy and deep learning study. *Analytical and Bioanalytical Chemistry* **2022**, *414* (3), 1297-1312. DOI: 10.1007/s00216-021-03749-y.

(62) Nigamatzyanova, L.; Fakhrullin, R. Dark-field hyperspectral microscopy for label-free microplastics and nanoplastics detection and identification in vivo: A Caenorhabditis elegans study. *Environmental Pollution* **2021**, *271*, 116337. DOI: https://doi.org/10.1016/j.envpol.2020.116337.

(63) Fournier, S. B.; D'Errico, J. N.; Adler, D. S.; Kollontzi, S.; Goedken, M. J.; Fabris, L.; Yurkow, E. J.; Stapleton, P. A. Nanopolystyrene translocation and fetal deposition after acute lung exposure during late-stage pregnancy. *Particle and Fibre Toxicology* **2020**, *17* (1), 55. DOI: 10.1186/s12989-020-00385-9.

(64) Rahman, L.; Mallach, G.; Kulka, R.; Halappanavar, S. Microplastics and nanoplastics science: collecting and characterizing airborne microplastics in fine particulate matter. *Nanotoxicology* **2021**, *15* (9), 1253-1278. DOI: 10.1080/17435390.2021.2018065.

(65) Bouwmeester, H.; Hollman, P. C. H.; Peters, R. J. B. Potential Health Impact of Environmentally Released Micro- and Nanoplastics in the Human Food Production Chain: Experiences from Nanotoxicology. *Environmental Science & Technology* **2015**, *49* (15), 8932-8947. DOI: 10.1021/acs.est.5b01090.

(66) Malafaia, G.; da Luz, T. M.; Ahmed, M. A. I.; Karthi, S.; da Costa Araújo, A. P. When toxicity of plastic particles comes from their fluorescent dye: a preliminary study involving neotropical Physalaemus cuvieri tadpoles and polyethylene microplastics. *Journal of Hazardous Materials Advances* **2022**, *6*, 100054.

(67) Lenz, R.; Enders, K.; Nielsen, T. G. Microplastic exposure studies should be environmentally realistic. *Proc Natl Acad Sci USA* **2016**, *113* (29), E4121-E4122. DOI: https://doi.org/10.1073/pnas.1606615113.

(68) Shen, M.; Zhang, Y.; Zhu, Y.; Song, B.; Zeng, G.; Hu, D.; Wen, X.; Ren, X. Recent advances in toxicological research of nanoplastics in the environment: A review. *Environmental Pollution* **2019**, *252*, 511-521. DOI: https://doi.org/10.1016/j.envpol.2019.05.102.

(69) Shruti, V. C.; Pérez-Guevara, F.; Elizalde-Martínez, I.; Kutralam-Muniasamy, G. First study of its kind on the microplastic contamination of soft drinks, cold tea and energy drinks - Future research and environmental considerations. *Science of The Total Environment* **2020**, *726*, 138580. DOI: https://doi.org/10.1016/j.scitotenv.2020.138580.

(70) Prata, J. C.; Paço, A.; Reis, V.; da Costa, J. P.; Fernandes, A. J. S.; da Costa, F. M.; Duarte, A. C.; Rocha-Santos, T. Identification of microplastics in white wines capped with polyethylene stoppers using micro-Raman spectroscopy. *Food Chemistry* **2020**, *331*, 127323. DOI: https://doi.org/10.1016/j.foodchem.2020.127323.

(71) Bern, L. Size-related discrimination of nutritive and inert particles by freshwater zooplankton. *Journal of Plankton Research* **1990**, *12* (5), 1059-1067. DOI: 10.1093/plankt/12.5.1059 (acccessed 11/8/2022).

(72) Adhikari, S.; Kelkar, V.; Kumar, R.; Halden, R. U. Methods and challenges in the detection of microplastics and nanoplastics: a mini-review. *Polymer International* **2022**, *71* (5), 543-551.

(73) Fu, W.; Min, J.; Jiang, W.; Li, Y.; Zhang, W. Separation, characterization and identification of microplastics and nanoplastics in the environment. *Science of The Total Environment* **2020**, *721*, 137561. DOI: https://doi.org/10.1016/j.scitotenv.2020.137561.

(74) Karami, A.; Golieskardi, A.; Choo, C. K.; Romano, N.; Ho, Y. B.; Salamatinia, B. A high-performance protocol for extraction of microplastics in fish. *Science of The Total Environment* **2017**, *578*, 485-494. DOI: https://doi.org/10.1016/j.scitotenv.2016.10.213.

(75) Scheurer, M.; Bigalke, M. Microplastics in Swiss Floodplain Soils. *Environmental Science & Technology* **2018**, *52* (6), 3591-3598. DOI: 10.1021/acs.est.7b06003.

(76) Nuelle, M.-T.; Dekiff, J. H.; Remy, D.; Fries, E. A new analytical approach for monitoring microplastics in marine sediments. *Environmental Pollution* **2014**, *184*, 161-169. DOI: https://doi.org/10.1016/j.envpol.2013.07.027.

(77) Karakolis, E. G.; Nguyen, B.; You, J. B.; Rochman, C. M.; Sinton, D. Fluorescent Dyes for Visualizing Microplastic Particles and Fibers in Laboratory-Based Studies. *Environmental Science & Technology Letters* **2019**, *6* (6), 334-340. DOI: 10.1021/acs.estlett.9b00241.

(78) Stanton, T.; Johnson, M.; Nathanail, P.; Gomes, R. L.; Needham, T.; Burson, A. Exploring the Efficacy of Nile Red in Microplastic Quantification: A Costaining Approach. *Environmental Science & Technology Letters* **2019**, *6* (10), 606-611. DOI: 10.1021/acs.estlett.9b00499.

(79) Fiore, L.; Serranti, S.; Mazziotti, C.; Riccardi, E.; Benzi, M.; Bonifazi, G. Classification and distribution of freshwater microplastics along the Italian Po river by hyperspectral imaging. *Environmental Science and Pollution Research* **2022**, *29* (32), 48588-48606. DOI: 10.1007/s11356-022-18501-x.

(80) Zhang, Y.; Wang, X.; Shan, J.; Zhao, J.; Zhang, W.; Liu, L.; Wu, F. Hyperspectral Imaging Based Method for Rapid Detection of Microplastics in the Intestinal Tracts of Fish. *Environmental Science & Technology* **2019**, *53* (9), 5151-5158. DOI: 10.1021/acs.est.8b07321.

(81) Piarulli, S.; Malegori, C.; Grasselli, F.; Airoldi, L.; Prati, S.; Mazzeo, R.; Sciutto, G.; Oliveri, P. An effective strategy for the monitoring of microplastics in complex aquatic matrices: Exploiting the potential of near infrared hyperspectral imaging (NIR-HSI). *Chemosphere* **2022**, *286*, 131861. DOI: https://doi.org/10.1016/j.chemosphere.2021.131861.

(82) Ai, W.; Liu, S.; Liao, H.; Du, J.; Cai, Y.; Liao, C.; Shi, H.; Lin, Y.; Junaid, M.; Yue, X.; et al. Application of hyperspectral imaging technology in the rapid identification of microplastics in farmland soil. *Science of The Total Environment* **2022**, *807*, 151030. DOI: https://doi.org/10.1016/j.scitotenv.2021.151030.

(83) Badireddy, A. R.; Wiesner, M. R.; Liu, J. Detection, Characterization, and Abundance of Engineered Nanoparticles in Complex Waters by Hyperspectral Imagery with Enhanced Darkfield Microscopy. *Environmental Science & Technology* **2012**, *46* (18), 10081-10088. DOI: 10.1021/es204140s.

(84) Théoret, T.; Wilkinson, K. J. Evaluation of enhanced darkfield microscopy and hyperspectral analysis to analyse the fate of silver nanoparticles in wastewaters. *Analytical Methods* **2017**, *9* (26), 3920-3928, 10.1039/C7AY00615B. DOI: 10.1039/C7AY00615B.

(85) Zamora-Perez, P.; Tsoutsi, D.; Xu, R.; Rivera_Gil, P. Hyperspectral-Enhanced Dark Field Microscopy for Single and Collective Nanoparticle Characterization in Biological Environments. *Materials* **2018**, *11* (2), 243.

(86) Botha, T. L.; Boodhia, K.; Wepener, V. Adsorption, uptake and distribution of gold nanoparticles in Daphnia magna following long term exposure. *Aquatic Toxicology* **2016**, *170*, 104-111. DOI: https://doi.org/10.1016/j.aquatox.2015.11.022.

(87) Pelegrini, K.; Pereira, T. C. B.; Maraschin, T. G.; Teodoro, L. D. S.; Basso, N. R. D. S.; De Galland, G. L. B.; Ligabue, R. A.; Bogo, M. R. Micro- and nanoplastic toxicity: A review on size, type, source, and test-organism implications. *Science of The Total Environment* **2023**, *878*, 162954. DOI: https://doi.org/10.1016/j.scitotenv.2023.162954.

(88) Shi, C.; Liu, Z.; Yu, B.; Zhang, Y.; Yang, H.; Han, Y.; Wang, B.; Liu, Z.; Zhang, H. Emergence of nanoplastics in the aquatic environment and possible impacts on aquatic organisms. *Science of The Total Environment* **2024**, *906*, 167404. DOI: https://doi.org/10.1016/j.scitotenv.2023.167404.

(89) Feldman, A. T.; Wolfe, D. Tissue Processing and Hematoxylin and Eosin Staining. In *Histopathology: Methods and Protocols*, Day, C. E. Ed.; Springer New York, 2014; pp 31-43.

(90) Dey, P. Haematoxylin and Eosin Stain of the Tissue Section. In *Basic and Advanced Laboratory Techniques in Histopathology and Cytology*, Springer Singapore, 2018; pp 69-79.

(91) Rodriguez-Seijo, A.; Lourenço, J.; Rocha-Santos, T. A. P.; da Costa, J.; Duarte, A. C.; Vala, H.; Pereira, R. Histopathological and molecular effects of microplastics in Eisenia andrei Bouché. *Environmental Pollution* **2017**, *220*, 495-503. DOI: https://doi.org/10.1016/j.envpol.2016.09.092.

(92) Zhou, X.; Wang, G.; An, X.; Wu, J.; Fan, K.; Xu, L.; Li, C.; Xue, Y. Polystyrene microplastic particles: In vivo and in vitro ocular surface toxicity assessment. *Environmental Pollution* **2022**, *303*, 119126. DOI: https://doi.org/10.1016/j.envpol.2022.119126.

(93) Gonçalves, C.; Martins, M.; Costa, M. H.; Costa, P. M. Development of a method for the detection of polystyrene microplastics in paraffin-embedded histological sections. *Histochemistry and Cell Biology* **2018**, *149* (2), 187-191. DOI: 10.1007/s00418-017-1613-1.

(94) Benito-Kaesbach, A.; Amigo, J. M.; Izagirre, U.; Garcia-Velasco, N.; Arévalo, L.; Seifert, A.; Castro, K. Misinterpretation in microplastic detection in biological tissues: When 2D imaging is not enough. *Science of The Total Environment* **2023**, *876*, 162810. DOI: https://doi.org/10.1016/j.scitotenv.2023.162810.

(95) Aramendia, J.; García-Velasco, N.; Amigo, J. M.; Izagirre, U.; Seifert, A.; Soto, M.; Castro, K. Evidence of internalized microplastics in mussel tissues detected by volumetric Raman imaging. *Science of The Total Environment* **2024**, *914*, 169960. DOI: https://doi.org/10.1016/j.scitotenv.2024.169960.

Appendix: Supplementary Information

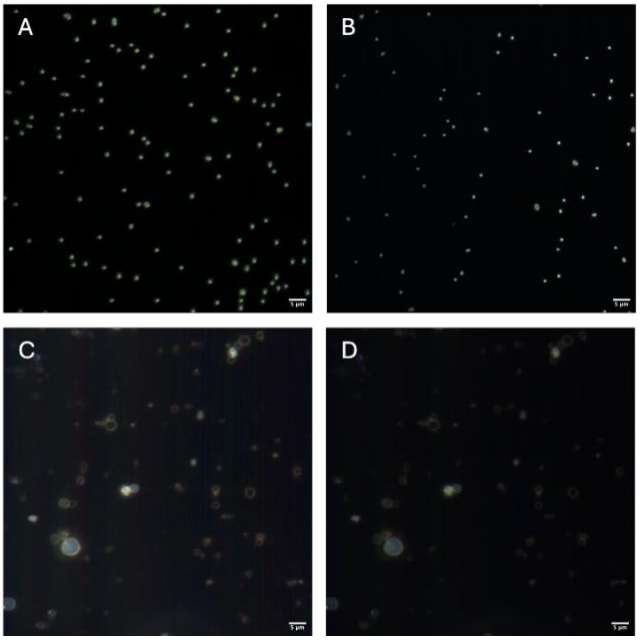

Figure S1. Reference image of plastic MNP. Fig. S1A contains 750 nm PS particles. Fig S 1B contains 500 nm PS particles. Fig S1C contains 200 to 9900 nm PE particles. This image has been altered by increasing the brightness by 50% for visualization purposes. Fig S1D is the raw, unaltered image of Fig. S1C.

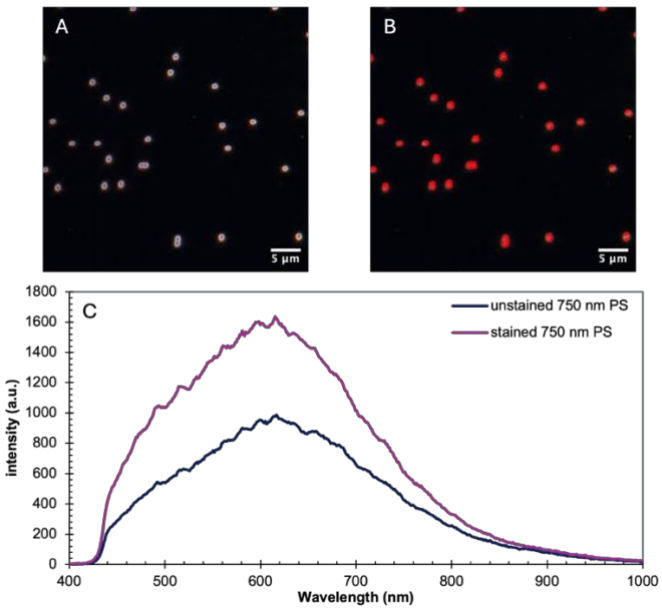

Figure S2. 750 nm PS particles stained with 25% H&E. Fig. S2A is the darkfield image of 750 nm PS particles after they have been stained with 25% H&E. Fig. S2B is the corresponding mapped image using the Spectral Angle Mapping tool, indicating all particles were detected. This proves that the 750 nm particles are not affected by the staining protocol and remain unlabelled. Fig. S2C shows the average spectrum of unstained and stained 750 nm PS. Here, the shape of the graph as well as the peak wavelength remain unchanged before and after staining. The peak wavelength of unstained PS is 616 nm and 615 nm after staining.

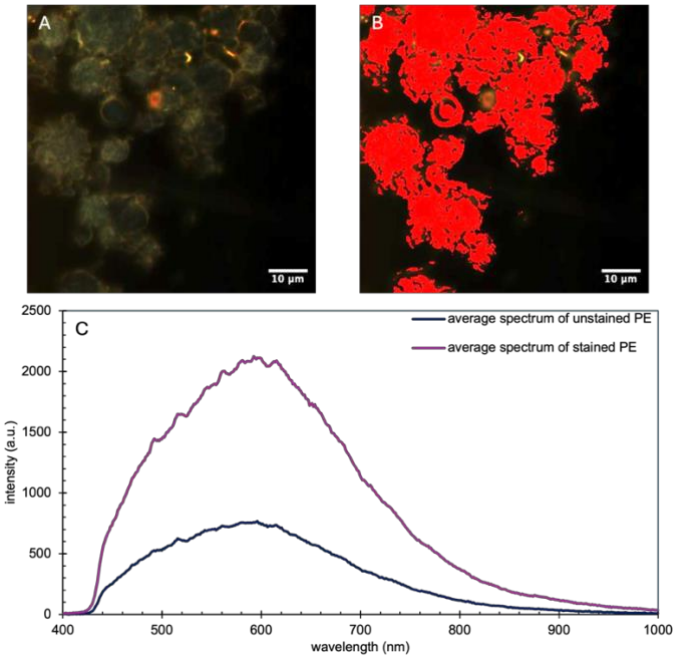

Figure S3. 200 to 9900 nm PE particles stained with 25% H&E. Fig. S3A is the darkfield image of the PE particles after they have been stained with 25% H&E. Fig. S3B is the corresponding mapped image using the Spectral Angle Mapping tool, indicating all particles were detected. The darkfield images were captured with half-field of view at 349 lines. Fig. S3C is a graph comparing the spectrum of unstained PE to the spectrum of PE after staining. The peak wavelength for unstained PE is 596 nm and the peak wavelength for stained PE is 592 nm.

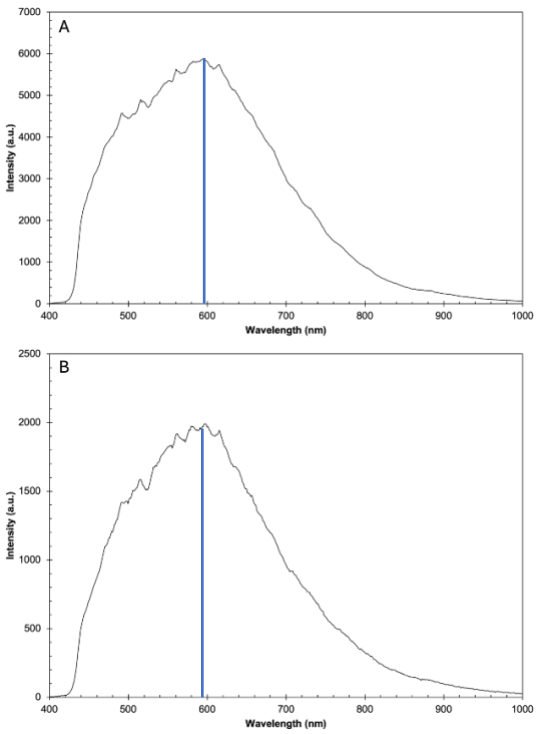

Figure S4. Comparing the average spectrum of a reference PS with PS within a histological slice. Fig. S4A is the average spectrum of a reference PS particle. Fig. S4B is the average spectrum of PS particles within a histological slice. The peak wavelength of reference PS particles is 594 nm, and peak wavelength of PS particles within a histological slice is 597 nm.

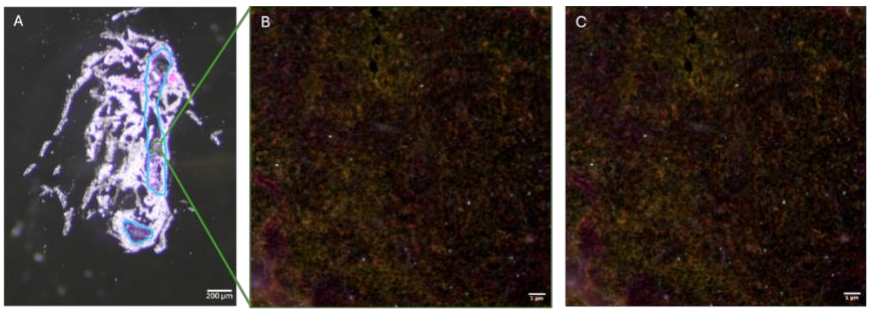

Figure S5. A control *D. magna's* gut was imaged. Fig. S5A is a darkfield image of a histological slice of the control sample. The gut region is outlined in blue. Fig. S5B is a darkfield image acquired on the EDF-HSI microscope of an area in the gut. Fig. S5C is the corresponding mapped image where it is evident SAM tool did not identify any MNP within the sample.

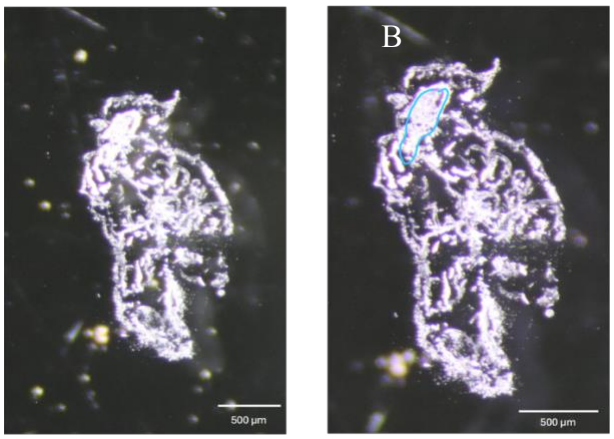

Figure S6. Darkfield images of the *D. magna* exposed to 750 nm PS at a concentration of 0.1 ppm. Fig. S6A is the darkfield image before staining. Fig. S6B is a darkfield image after 25% H&E staining. A part of the gut region is outlined in blue.

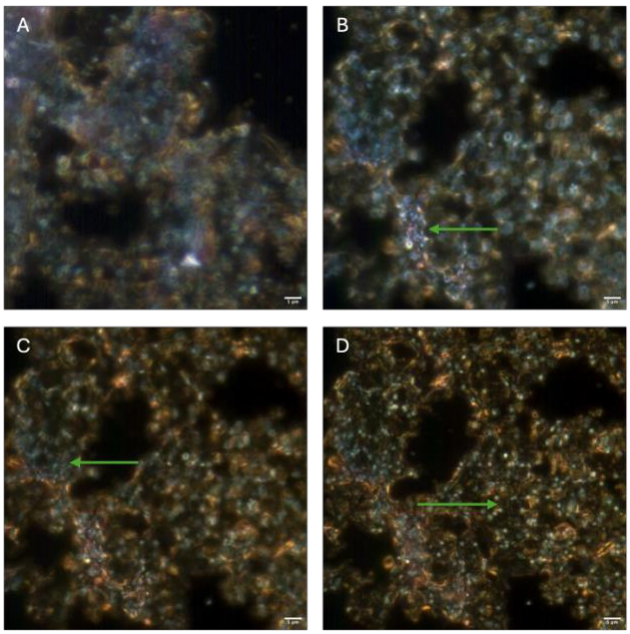

Figure S7. Darkfield images at various focal depths to acquire a "z-stack". Fig. S7A is the first image in the stack where everything is out of focus. Fig. S7B focuses on a few particles shown with the green arrow. Fig. S7C and D focus on more particles shown with a green arrow on each respective image. The *D. magna* was exposed to 750 nm PS at a concentration of 0.1 ppm.

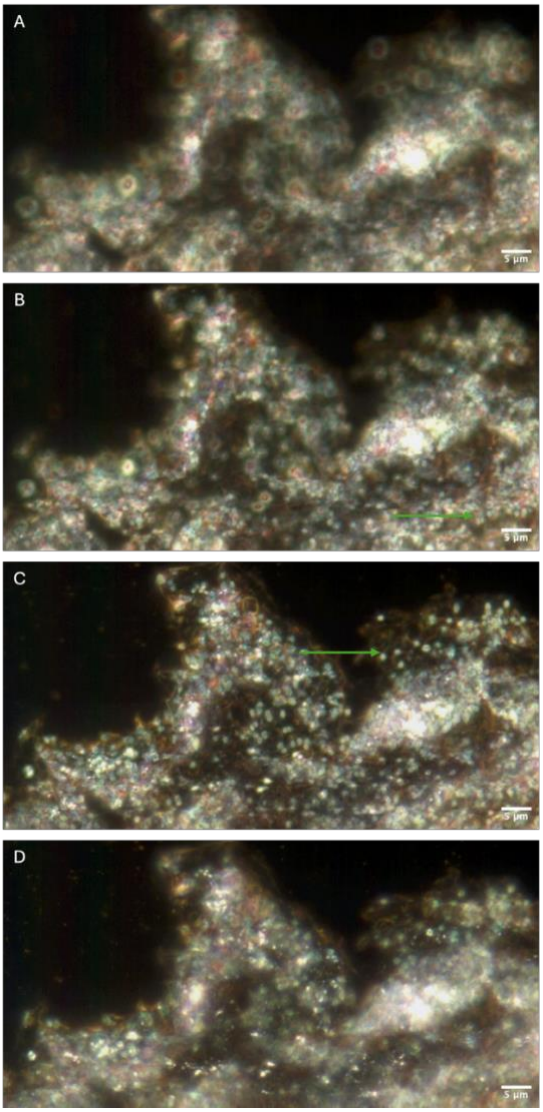

Figure S8. Images at various focal depths to acquire a "z-stack". Fig. S8A is the first image in the stack where everything is out of focus. Fig. S8B and C focus on more particles shown with a green arrow on each respective image. Fig. S8D is the last image where most of the image is out of focus. The *D. magna* was exposed to 750 nm PS at a concentration of 0.1 ppm. The darkfield images were captured with half-field of view at 349 lines.

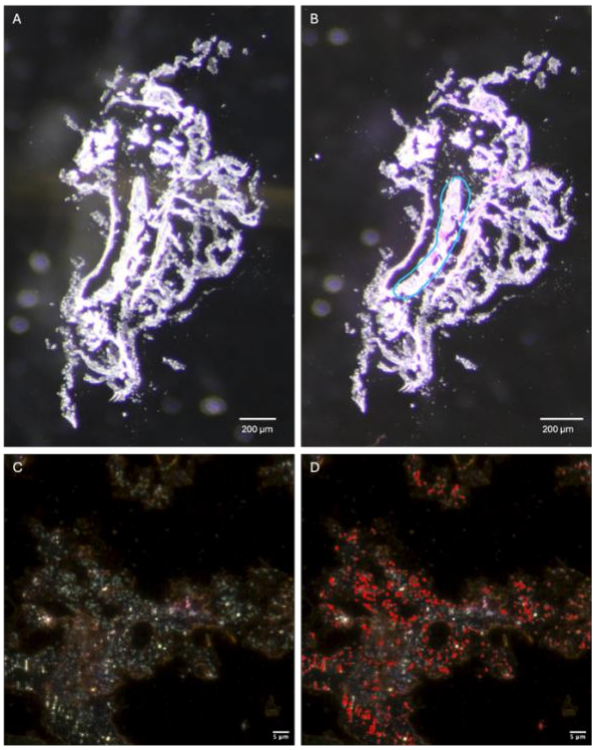

Figure S9. Detection of 500 nm PS at 0.01 ppm within the gut of *D. magna.* Fig. S9A is the darkfield image of a histological slice of the *D. magna* before staining. Fig. S9B is the darkfield image of a histological slice of the *D. magna* after staining. The gut region is outlined in blue. Fig. S9B is the darkfield image of one area of the gut acquired on the EDF-HIS. Fig. S9D is the corresponding mapped image, where 500 nm PS particles have been detected in red.

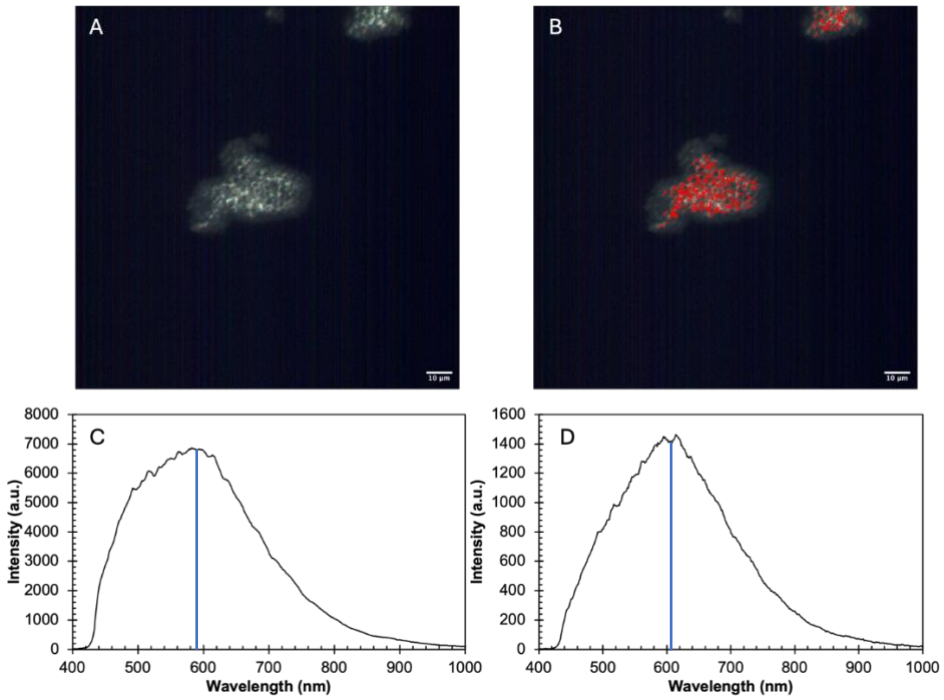

Figure S10. Images of UV-weathered 3 µm PS. Weathering took place over a span of 45 days in a UV chamber temperature of 25 °C. Fig. S10A is a darkfield image of the weathered microplastic. Fig. S10B is the corresponding mapped image using the Spectral Angle Mapping tool. Fig. S10C is the average spectra of pristine 3 µm PS. Fig. S10D is the average spectra of the weathered 3 µm PS. The complete mapping of focused microplastics in Fig. S10B indicate that the spectra of microplastic does not change after weathering, which is supported by the shape of the average spectrum before and after weathering remaining the same. The peak wavelength of pristine 3 µm PS is 582 nm, whereas the peak wavelength of weathered 3 µm PS is 613 nm.